"Synthesis and Characterization of Piezoelectric and Piezoelectric-Multiferroic Composite Thin Films for MEMS Applications"

A

Thesis Submitted

for the Award of Degree of

Master of Technology (M-Tech)

By

Mintu Tyagi

(600902006)

Submitted to

Thapar University, Patiala (Punjab)

Under the Supervision of

Dr. Puneet Sharma

School of Physics & Material Science

Thapar University, Patiala (Punjab)

Prof. Ratnamala Chatterjee

Department of Physics,

Indian Institute of Technology, Delhi

This Thesis is Dedicated

TO

MY PARENTS,

BROTHER AND SISTER

EVERTHING FOR ME

CERTIFICATE

This is certify that the work embodied in this thesis entitled **"Synthesis and Characterization of Piezoelectric and Piezoelectric-Multiferroic Composite Thin Films For MEMS Applications"** is being submitted by Mr. Mintu Tyagi in fulfillment of the requirement for the award of degree of M. Tech (Material Science and Metallurgical Engineering) from School of Physics and Material Science, Thapar University, Patiala is a record of candidate's own work carried out by him under my supervision and guidance the matter presented in this thesis has not been submitted in part or full for the award of my degree in any other university or institute for any other degree or diploma course.

Date:

Place:

15/07/11

Dr. Puneet Sharma

School of Physics and Material Science,

Thapar University, Patiala (Punjab), India

28/06/2011

Prof. Ratnamala Chatterjee

Department of Physics

Indian Institute of Technology, Delhi

Countersigned by

Dr. O.P. Panday

Prof. and Head (School of Physics and Material Science) Thapar University, Patiala, Punjab

S.K. Mohapatra

Dean, Academic Affairs

Thapar University, Patiala, Punjab

Table of Contents

Chapter 2: Ceramic Technologies at a Glance (Bulk and Thin Films)

Chapter 3: Experimental Methods

Chapter 4: Results and Discussion of $PbZrTiO_3$ Thin Films

List of Figures

Chapter 1

Chapter 3

Chapter 4

Chapter 5

ABSTRACT

The lead-zirconate-titanate (PZT) solid solutions system is currently the workhorse of piezoelectric-based microelectromechanical systems (MEMS) research. Among bulk material it is known to be one of the strongest piezoelectric, with extremely high piezoelectric coefficients and electromechanical coupling factor. Reproducing these properties in thin film form, however, require precise control of composition and texture. in this thesis, method to grow textured or epitaxial PZT thin film are investigated. The aim is to develop maximize crystallinity and minimize resistivity through precursor modification and thermal treatments**.**

Lead zirconate titanates (PZTs and PLZTs) are being used in bulk as well as in thin film forms for various applications like transducers, actuators and FERAMs for civil and military applications. The piezoelectric and electro mechanical property of these materials are excellent inspite of their toxic behavior and have always attracted the researchers for its maximum exploitation. The bulk PZTs are extensively used for under water and ultrasound applications. The commercial uses of these compounds are in inkjet printers, precise cutting machines and many other vibrators. The thin films of these materials can be used for making vibration sensors, MEMS (Micro Electro Mechanical Systems) switches etc. The preparation and characterization of ferroelectric/piezoelectric in bulk and thin film forms of PZT with suitable substituent's are presented in this thesis. After a brief introduction to ferroelectric/piezoelectric materials and their studies done in the past the thesis starts with defining the objectives and scope of the present work. Since our aim was to make thin films of PZT on platinized silicon substrates, it was important to look at their lattice parameters for minimum lattice mismatch. In this research the platinized silicon substrate of 1500 Å platinum thickness substrates have been used for thin films study. Further platinum <111> has a lattice constant ~ 3.92 Å. Thus a PZT system which can be more suitable near MPB of $PbZrO_3$ – $PbTiO_3$ will be none other than the PZT with a molar Zr/Ti ratio of 52/48 whose lattice constant is also ~ 4 Å. These literature results were primary basis for the present research. Thus this particular Zr/Ti ratio of 52/48 was chosen for further study. Furthermore a high value of remnant polarization has been observed for the PZT (52/48) bulk ceramics. Hence for making a thin film of the same composition based devices like (FERAM, MEMS based vibration

sensors etc.), it would be interesting to deposit thin films of PZT on suitable substrates. A systematic study had been planned to investigate the structural, morphological and electrical properties of these ceramics in bulk and thin films.

Chemical solution deposition (CSD) and physical vapor deposition (PVD) technique were also used to optimize orientation in PZT thin films. A comprehensive investigation of lead chemistry as well as pyrolysis and annealing conditions was performed to determine the processing-structure-property relationships in PZT films. in concert, sputtering methods were also developed for comparison of thin films PZT properties from PZT and CSD method.

It is expected that these films will offer enhanced piezoelectric actuation due to their high degree of orientation, relatively small amount of high-angle grain boundaries and their superior ferroelectric characteristics. Additionally, the flexibility of substrate open doors to many exiting materials integration possibilities for MEMS devices including energy harvesting applications and flexible sensor.

CHAPTER 1

INTRODUCTION

The field microelectromechanical systems or MEMS is rapidly expanding for sensing, actuation and even energy harvesting. Currently, MEMS have made headway as actuators for ink jet printer, accelerometers, gyroscopes and as many other types of sensors some of which can power themselves by capturing ambient mechanical or thermal energy. The development of MEMS devices has benefited from 50 years of integrated circuit manufacturing expertise but an understanding of the thin film materials used to make them is much more recent. Knowledge of the electrical, piezoelectric and mechanical properties of materials is crucial to MEMS design. Specifically, ways to maximize displacement and actuation with low hysteresis and power requirements are desired. Piezoelectric materials offer these advantages to MEMS researchers.

To develop piezoelectric materials with large amplitude actuation, however, a thorough understanding of the materials structure-property relationships is required. The piezoelectric *d* coefficients, which describe displacement per volt in a specified direction, are dependent on the films composition and crystallographic texture. These parameters can be precisely tuned through processing conditions. A great deal of progress has been made in understanding these interrelated processing structure property relationships in the most widely used piezoelectric thin film, the Pervoskite Pb(Zr,Ti)O3. The lead-zirconate-titanate (PZT) solid solution system possesses unusually high piezoelectric coefficients, which are highly influenced by composition and texture. In this thesis, methods of enhancing PZT film texture through substrate selection and processing variables are investigated.

1.1: Brief Overview.

In the past several decades extensive work has been done on Lead Zirconate Titanates (PZTs) and lanthanum (La^{3+}) substituted PZTs (PLZT) [1-6]. These compositions are finding many applications in a variety of sensors and actuators based on both bulk and micro electro mechanical systems (MEMS) due to their (i) higher electromechanical coupling coefficients compared to $BaTiO_3$, (ii) higher T_c, (iii) easy to pole, (iv) a wide range of dielectric constants, (v) are relatively easy to sinter at lower temperatures than $BaTiO_3$, and (vi) form solid-solution compositions with many different constituents giving wide range of achievable properties [4]. Properties of PZT can be

tailored by suitable substitution to achieve material with desired characteristics for a targeted application. Examples of these additives include off-valent donors, such as Nb^{5+} replacing Zr^{4+} or La^{3+}/Sm^{3+} replacing Pb^{2+} to counteract the natural *p*-type conductivity of the PZT and thus increase the electrical resistivity of the materials by at least 3 orders of magnitude. The donors are usually compensated by A-site vacancies. These additives/substituent's (and vacancies) enhance domain reorientation in ceramics and which in turn results in square hysteresis loops, low coercive fields, high remnant polarization, high dielectric constants, enhanced coupling factors, higher dielectric loss, high mechanical compliance and reduced aging. Apart from the transducer applications in bulk form, Ferroelectric/Piezoelectric thin films have attracted a the attention of researchers due to its potential for many important device applications such as: high value capacitors, infrared detectors, SAW- delay lines, sensors and actuators, optical switches, electro-optic devices, non volatile random access memories etc. [7-15]. More precisely thin piezoelectric films are being used in pressure sensors, vibration sensors, SAW devices, bulk acoustic resonators, accelerometers, gas sensors, chemical sensors, infrared sensors and actuators and biosensors also [16-20].

For piezoelectric thin film based devices, a key processing challenge is to prepare a piezoelectric thin film with the desired structure and properties. It is a requirement that these films should be stable, uniform in their chemical composition and physical properties, and should be reproducible. PZT films are required to be prepared in pure Pervoskite (ferroelectric) phase for their best piezoelectric response. Also, the resistivity of these films should be high. Furthermore, the film deposition should be optimized at comparatively low temperature so that they can be used more effectively while making devices where numerous processing and etching steps are involved. Various techniques are being used for the deposition of PZT films, such as sputtering, evaporation, chemical vapour deposition, sol-gel, spray pyrolysis, pulsed laser deposition, atomic layer deposition, vacuum arc deposition and molecular beam epitaxial [21, 22]. Among these pulsed laser deposition and sol gel techniques are the most attractive ones for preparing these films. While the sol gel technique has the advantage that the composition of the film (as in the case of PZT) can be easily tailored for optimum performance [23], the laser ablation technique is an state of the art technique with a number of advantages like

(a) stoichiometric film, (ii) congruent ablation and controlled high deposition rate etc. Preparation of thin films of PZT in pure perovskite (ferroelectric) phase is a challenging task. A common problem comes from the lead loss due to high deposition temperature [24]. The resulting non-stoichiometric of the films leads to the formation of the pyrochlore phases, which degrade the film properties. Typically while depositing thin films by laser ablation, excess lead (up to 40%) is added into the target to compensate for lead volatilization during thin film deposition process [25]. Also, for minimizing lead loss, efforts are made so that these films are deposited at a relatively lower temperature, and then post deposition treatment is given by annealing at higher temperature [26]. The formation of pyrochlore phase also arises due to the deficiency of oxygen in the film [27]. Therefore, it is essential to study the effect of various deposition parameters, mainly deposition temperature, oxygen partial pressure for the films being deposited in reactive environment and post deposition annealing temperature, on the phase stabilization of the films.

Since the present work aims at study of optimized piezoelectric material in the bulk form that can be transformed easily onto substrates to make thin films. For this purpose the piezoelectric material composition chosen was PZT with Zr/Ti ratio as 52/48 [4]. This composition is well for good electrical properties have been optimized. The substrates used were platinized silicon. Platinum <111> has a lattice constant ~ 3.92 Å. Thus a PZT system which can be more suitable of $PbZrO_3$ – $PbTiO_3$ system will be none other than the PZT with a molar Zr/Ti ratio of 52/48 whose lattice constant is also ~ 4 Å [28]. These literature results are the primary basis for the present undertaken research. The reason for choosing this particular composition was its minimum lattice mismatch with the Pt (Pt/Si) substrate while depositing the same composition of the bulk in thin films.

Sol-gel processing of thin-layer dielectrics in lead titanate based systems was done by Budd et.al [29]. Thin-layer dielectrics were prepared by spin-casting methods. Details are given for the sol-gel process. Dense amorphous layers were formed at 300^oC, and crystallization occurred above 450^oC. The electric field strengths were in excess of 200 kV/cm. Values of dielectric constant ranged from 30 for amorphous layers to 1700 for polycrystalline PZT (48/52). PZT 48/52 was ferroelectric with a remnant polarization of $32.5\mu C/cm^2$. An electro-optic effect was demonstrated in a PZT optical switch.

Preparation and properties of PZT films from metallo-organic precursors was reported by Vest et al [30]. Crack free and dense PZT (48/52) films were prepared by spinning a solution of metallo-organic compounds of lead, lanthanum, zirconium and titanium onto sapphire substrates, and firing and annealing the films in air in the range 600 to 850^{o}C. These firing temperatures resulted in films with grain sizes from 0.2 to 1.2 μm. Films fired at 650^{o}C had a dielectric constant of 1800 and a dissipation factor of 2% at 1 kHz, and a spontaneous polarization of 5 μC/cm^{2}. Band Gap and Band tailing behavior of PZT thin films were reported by Khodorov et al [31]. The strong shift of the absorption edge in thin films in comparison with bulk PZT was observed. This shift could not be caused just by the presence of the strain. The increased disorder and polarization fluctuations were suggested as the additional reason that was supported by nearly twice higher value of the exponential tail width in the films in comparison with bulk PZT. Effect of processing conditions on the piezoelectric properties of sol-gel derived PZT films for micromechanical applications has been reported by Pérez et al.[32]. The films were annealed at lower temperature (500^{o}C). The maximum values of the longitudinal charge and voltage piezoelectric coefficients obtained were d_{33} ~ 65 pm/V and g_{33} ~ 4 × 10^{-3} Vm/N respectively.

1. 2.1 Ferroelectricity and piezoelectricity in crystals

Ferroelectricity and piezoelectricity in crystals can be explained on the basis of symmetry operations. It is found that symmetry operations can be combined in 32 different ways, resulting in 32 different crystal classes. Out of these 32, only eleven crystal classes have center of symmetry and 21 have non-centro symmetry. Further out of the remaining 21 non centro-symmetric, only 20 show pies' electricity. The remaining one non-centro symmetric class left does not show any piezoelectric effect because of the combined effect of symmetry. Piezoelectric effect is the phenomenon of creation of electric polarization on the application of external stress and vice-versa. Out of these 20 piezoelectric crystals only 10 posses spontaneous polarization. They are also known as pyroelectric crystals. Pyroelectric effect is the appearance of an electric charge at the surface of the material with change in ambient temperature. Further a current is generated when they are heated or cooled. These currents are generated due to these electrical

charges and are called pyroelectric current. Ferroelectricity appear only in few crystal classes out of 10 pyroelectric classes. Ferroelectricity is defined as electrically switchable polarization in crystals. These crystals show large dielectric constant and high coupling factor. Polycrystalline ceramics of these materials show ferroelectric effect only after poling or aligning the dipoles.

1.2.2 Ferroelectric Curie Point / Phase Transition Temperature

Usually at a well-defined temperature, crystal structure changes. This change is known as phase transition and the temperature at which the ferroelectric material changes its structure is called ferroelectric Curie point. At this point there is a change in the orientation or magnitude or both of the electric polarization. Crystals are no longer polar after this temperature. Dielectric constant is also maximum at Curie point. At this point spontaneous polarization vanishes as it approaches highly symmetric cubic phase. When the temperature decreases through the Curie point, the ferroelectric crystals further undergo a structural phase transition from paraelectric phase to a ferroelectric phase. For $T > T_{c,}$ dielectric constant decreases very rapidly according to Curie – Weiss's law :

i.e $$\varepsilon' = C / (T-T_c) \qquad \text{……(1.1)}$$

Where ε' is dielectric constant, C is Curie constant and T_c is the Curie – Weiss's temperature, which defines the paraelectric phase. This relation is in analogy with ferromagnetism. This anomaly in the dielectric behavior of ferroelectric materials with temperature is a main feature of ferroelectric materials. Definite proof of Ferroelectricity is the hysteresis loop and dielectric anomaly.

1.2.3 Piezoelectricity

The production of charge at the surface of the material specimen when subjected to mechanical stress or vice versa is known as piezoelectric effect. Curie brothers in 1880 observed that there is ability in some crystalline materials to develop an electric charge when they are subjected to some mechanical stress. It was also observed that the charge so developed is proportional to the applied mechanical stress. This effect is known as direct piezoelectric effect (designated as generator) and when an electric field is applied across the material specimen then there is a deformation or stress in the material. The

later effect is known as converse effect and is designated as motor. Further if the strain is proportional to the square of the applied field then the effect is known as electrostrictive effect. In a direct piezoelectric effect,

$$T = YS \qquad \ldots\ldots\ldots\ldots (1.2)$$

where T is stress, S is strain and Y is modulus of elasticity. Also some charge is created when stress is applied. It is of opposite sign for compression and expansion.

1.2.4. Piezoelectric Charge Coefficient (d)

When a piezoelectric material is subjected to stress, electric charge is generated on the surfaces. The charge generated per unit force is called piezoelectric charge coefficient and is denoted by 'd' which is measured in pC/N. Piezoelectric charge coefficient is a directional property and is usually specified with subscripts to identify the conditions under which it is determined e.g., d_{33} and d_{31}. In these piezoelectric charge coefficients, first subscript corresponds to the direction of the applied stress and second corresponds to the direction of the faces of the ceramic on which charges are developed.

The piezoelectric coupling factors (k_{33}, k_{31}) used for measurement of the strength of piezoelectric effect. If equal stress is applied along one and two directions then coupling factor is called planer coupling factor k_p. k_t refers to thickness coupling factor (in clamped plates).

1.2.4. Hydrostatic charge Coefficient (d_h)

It corresponds the effect of development of charge when a pressure is applied on the material. Hydrostatic charge coefficient (d_h) is related to d_{33} and d_{31} piezoelectric charge constants by the relation and is measured in Coulomb/Newton (C/N) units.

$$d_h = d_{33} + 2d_{31} \qquad \ldots\ldots\ldots\ldots\ldots\ldots (1.3)$$

1.2.5. Piezoelectric Voltage Constant (g)

It gives the field produced by a stress in a piezoelectric material. Its usual units are meter volts / Newton and 'g' constant is related to the'd' constant by the permittivity

$$g = d / (\varepsilon' \varepsilon_o) \qquad \ldots\ldots\ldots\ldots 1.4$$

Where g is called the piezoelectric voltage coefficient and ε_o are the dielectric constant of the material and permittivity of the free space, respectively. Corresponding to d_{33} and d_{31} piezoelectric constants, there exist g_{33} and g_{31} piezoelectric voltage coefficients.

1.2.6. Hydrostatic Voltage Coefficient (g_h)

It gives the field produced by a pressure. It is related to the g_{33} and g_{31} piezoelectric charge coefficients by the relation and its usual units are meter volts/Newton.

$$g_h = g_{33} + 2g_{31} \qquad \ldots\ldots 1.5$$

1.2.7. Electromechanical Coupling Factor (k)

Most powerful measurement of the strength of the piezoelectric effect is the electromechanical coupling factor k, which reflects the efficiency of a material. It gives us the measure of the part of the applied electrical energy converted into mechanical energy or vice-versa and measured by resonance method [24].

$$k^2 = \frac{\text{Mechanical energy converted into electrical energy}}{\text{Input Mechanical energy}} \qquad (1.6)$$

Or

$$k^2 = \frac{\text{Electrical energy converted into mechanical energy}}{\text{Input electrical energy}} \qquad (1.7)$$

Depending on the mode of energy conversion, there exist various electromechanical coupling factors like k_p, k_t and k_{33}. Here, k_p is planar coupling coefficient, related to the energy conversion, when the applied electric field is perpendicular to the generated mechanical vibrations, which are along the plane. k_t is

thickness coupling factor related to the energy conversion, when the applied electric field is in the direction of generated mechanical vibrations and which are along the thickness in the material. Large k_t and small k_p in a piezoelectric material exhibits huge anisotropy behavior. Due to large anisotropy, transverse modes get suppressed resulting in the prevention of pickups due to transverse mode.

1.3. Structure and Properties of PZT

1.3.1. Pervoskite Structure:

A type of ionic crystal structure shown by compounds of the type **ABO_3.** There is a cubic arrangement with A atomic surrounded by 12, O atoms and B atom surrounded by 6 O atoms. Example of the Pervoskite structure includes PZT (Lead Zirconium Titanium oxide), BF (Bismuth ferrite) and LF (Lanthanum ferrite).

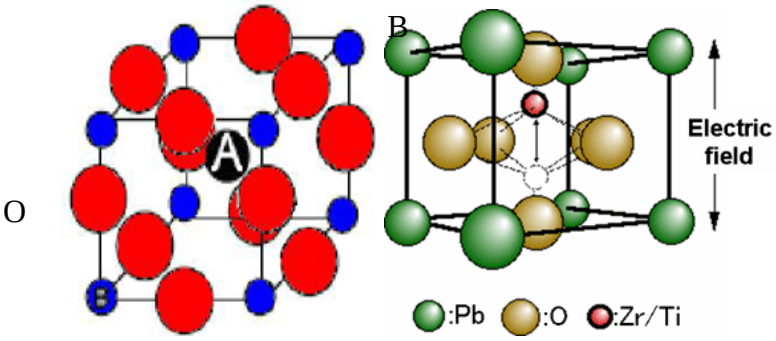

Fig.1.1 (a) Fig. 1.1 (b) Fig.1.1(c)

Fig.1.1 (a), (b) and (c) represent the atomic arrangement of the pervoskite structure (ABO_3), where 'A' and 'B' are two cations of different size, and 'O' is an anion that bond to both. The 'A' atoms are larger than the 'B' atoms. The ideal cubic-symmetry has the 'A' cation in 12-fold sub-octahedral coordination (Fig 1.1 (a)) and the 'B' cations in 6 fold coordination (Fig 1.1 (b)) surrounded by an octahedral of anions.

1.3.2. Phase diagram of {Pb ($Zr_{.52}Ti_{.48}$) O3}

The phase diagram of the PZT system (shown in Fig. 1.2) provides a useful way to classify the behavior of PZT [33]. A continuous solid solution exists between $PbTiO_3$ and $PbZrO_3$ as shown in the figure. Pure $PbTiO_3$ *has the tetragonal perovskite structure and is ferroelectric in nature. The compositions* rich in $PbTiO_3$ exhibit a ferroelectric tetragonal structure (FE_{Tet}) while the compositions rich in $PbZrO_3$ exhibit a ferroelectric

rhombohedral structure. A morphotropic phase boundary (MPB) separates the tetragonal phase from the rhombohedral phase (FE_{Rh}). Pure $PbZrO_3$ has an orthorhombic structure and is antiferroelectric in nature. The tetragonal and rhombohedral structures are known

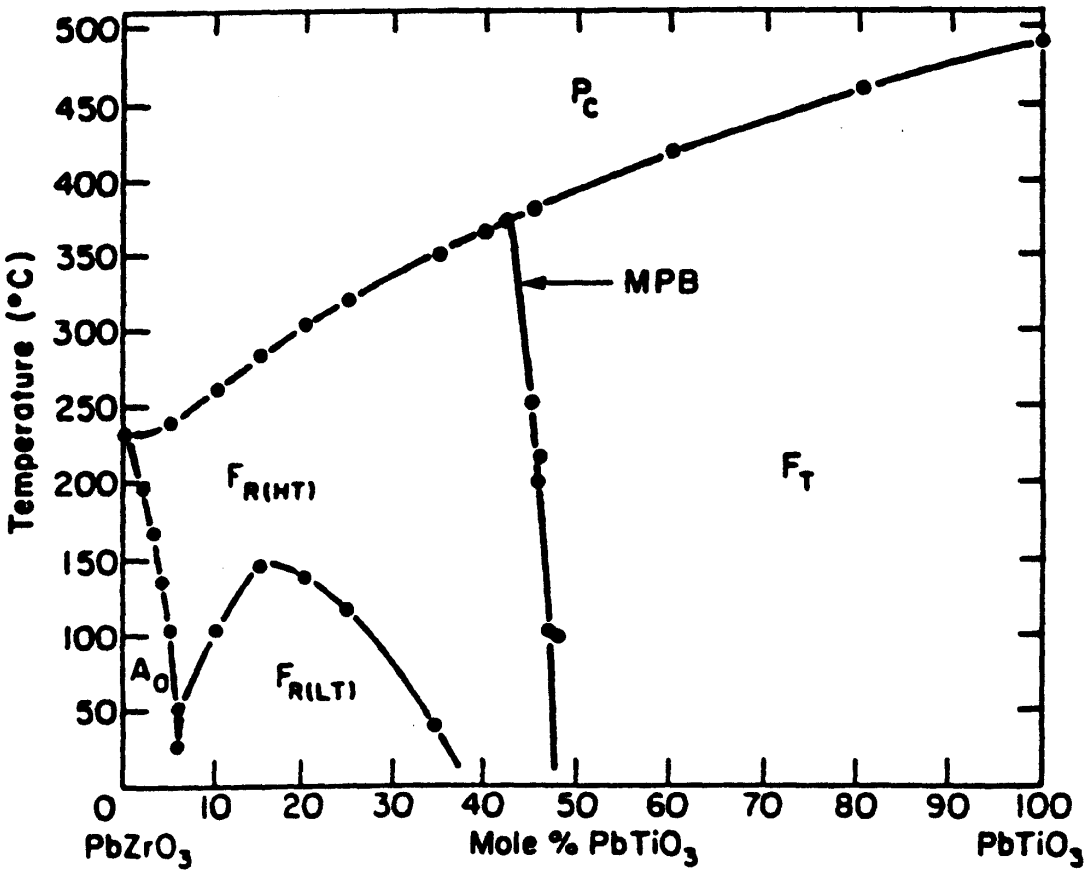

Figure 1.2

to exhibit ferroelectricity, the cubic phase shows paraelectric and the orthorhombic phase exhibits antiferroelectricity.

1.4. Multiferroics:

1.4.1. Introduction to Multiferroics

As the name suggests **multiferroic materials** posses more than one of the so called ferroic (ferroeletricity /ferromagnetism / ferroeleasticity) properties. In recent years this term is loosely used for the materials in which magnetism and Ferroelectricity coexist. The coexistence of these properties is reported in literature for single phase as

well as multiphase composite materials [5-17]. In 1894, P.Cuire predicted [3] that crystals could be simultaneously ferromagnetic and ferroelectric. The magnetization in the crystal can be induced by the application of electric field and vice versa. This effect is known as "**magneto electric effect**" and the coupling between ferroelectric and magnetic interactions is known as "**magneto electric coupling**". It is clear from the definition of magneto electric coupling that the coexistence of ferroelectric and ferromagnetic orders is a necessary condition for the material to be classified as a magneto electric material; however, magneto electric coupling is an independent phenomenon that need not arise in all materials that are both magnetically and electrically polarizable. In practice, it is likely to arise in all materials that are both magnetically and electrically polarizable, either directly or via strain. This concept is pictorially depicted by several authors [14, 17] through a schematic drawing as shown in Fig.1.3. In this diagram, ferromagnets (ferroelectrics) form a subset of magnetically (electrically) polarizable materials such as paramagnets and antiferromagnets (paraelectrics and antiferroelectrics) shown by dark circles (black and green). The intersection (red hatching) represents materials that are multiferroic and the blue hatching represents the materials that would show magnetoelectric coupling. The materials which have coexistence of ferroelectric and magnetic orders and exhibit magnetoelectric coupling are called "**Magnetoelectric Multiferroics**".

The magnetoelectric effect in a single phase crystal is traditionally described in Landau's theory [10, 11] by writing the free energy of the system in terms of applied magnetic and electric fields. For ferroic materials it is given by; In the above equation the second and third terms represent the spontaneous polarization (for ferroelectric material) and spontaneous magnetization (for ferromagnetic materials) respectively. The fourth (and fifth) terms describe the contribution resulting from the electrical (and magnetic) response to an electric field (and magnetic field). The permittivity (and permeability) of free space is given by ε_0 (and μ_0) and the relative permittivity ε_{ij} (T) (and relative permeability μ_{ij}) is a second rank tensor typically independent of applied electric field (and magnetic field). The tensor $\alpha_{i\ j}$ (T) corresponds to induction of polarization by a magnetic field or of magnetization by an electric field which is designated as **linear**

magnetoelectric coupling coefficient. The third order tensors β_{ijk} (T) and γ_{ijk} (T) repersent higher order magnetoelectric coupling coefficients.

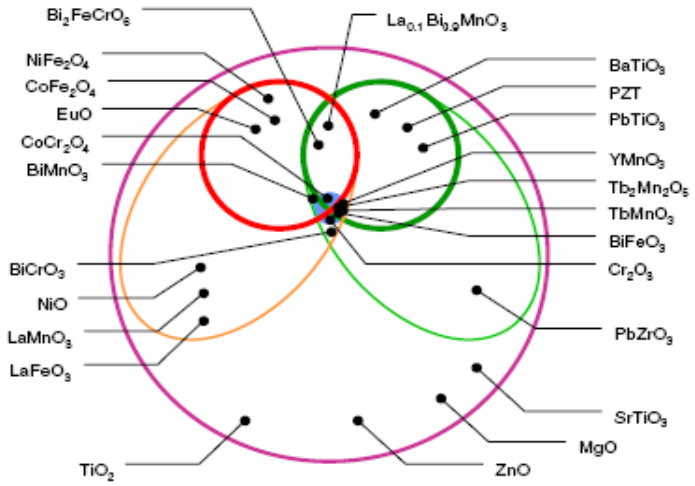

Fig.1.3 Relationship between multiferroic and magnetoelectric materials [17].

$$F(\vec{E},\vec{H}) = F_0 - P_i^S E_i - M_i^S H_i - \frac{1}{2}\varepsilon_0\varepsilon_{ij}E_iE_j - \frac{1}{2}\mu_0\mu_{ij}H_iH_j - \alpha_{ij}E_iH_j - \frac{1}{2}\beta_{ijk}E_iH_jH_k - \frac{1}{2}\gamma_{ijk}H_iE_jE_k ..... \quad (1.8)$$

The magnetoelectric effect can easily be established in the form of polarization P_i (H_j) and magnetization M_i (E_j). Differentiation of equation (1.1) with respect to E_i leads to polarization

$$P(\vec{E},\vec{H}) = -\frac{\partial F}{\partial E_i} = P_i^S + \varepsilon_0\varepsilon_{ij}E_j + \alpha_{ij}H_j + \frac{1}{2}\beta_{ijk}H_jH_k + \gamma_{ijk}H_iE_j - ..... \quad (1.9)$$

The term P_i^S denotes the spontaneous polarization. By setting the electric field term to zero in equation (1.2) we get

$$P_i(H_j) = \alpha_{ij}H_j + \frac{1}{2}\beta_{ijk}H_jH_k .....$$

Similarly the differentiation of equation (1.1) with respect to H_i gives magnetization

$$M_i(\vec{E},\vec{H}) = -\frac{\partial F}{\partial H_i} = M_i^S + \mu_0\mu_{ij}H_j + \alpha_{ij}E_i + \beta_{ijk}E_iH_j + \frac{1}{2}\gamma_{ijk}E_jE_k - ..... \quad (1.10)$$

where the term M_i^S represents spontaneous magnetization. By setting the magnetic field term zero in equation (1.4) we get

(1.11)

$$\mu_0 M_i(E_j) = \alpha_{ij} E_i + \frac{1}{2}\gamma_{ijk} E_j E_k - .....$$

Clearly, from above equations (1.3 and 1.5),

$$\alpha_{ij}^2 \leq \chi_{ij}^{electric} \chi_{ij}^{magnetic} \qquad \text{……..... (1.12)}$$

Where $\chi_{ij}^{electric}$ and $\chi_{ij}^{magnetic}$ are electric and magnetic susceptibilities respectively. In 2004, Gong *et al.* [18] theoretically predicted that if two transition temperatures *i.e.* ferroelectric transition temperature and ferromagnetic transition temperature occur very close to each other; large magnetoelectric coupling is expected in that temperature range In this field great progress has been made and people have made the materials possessing both electric and magnetic properties simultaneously (**magneto electric effect)** [1-3]. This has created a great interest for research as both properties in single materials has huge application in coming future.

"It was the initially suggest that both magnetization and polarization could independently encode information in single multiferroic bit. Coupling of magnetic and electric properties in principle permit data to be written electrically and read magnetically. This feature would exploit the best aspect of ferroelectric random access memory (FeRAM) and magnetic data storage, while avoiding the problems associated with reading FeRAM and generating the large local magnetic field needed to write." [4]

Research is trying their best to obtain the **coupling effect in** new materials and enhance the coupling effect in materials. As the theory predicts that such materials rarely exist and some stringent condition has to satisfied their existence add more difficulty in fabrication these materials.

Among the various methods use for Preparation of multiferroic thin film, **SOL-GEL** [9, 10] method is most acclaimed method because of it's great ease and simplicity. It has a lot of advantage over other methods and rather it has got certain disadvantage too. We have use SOL-GEL method for Preparation of sample thin film. Thin film has been deposited by spin coating method.

Finally characterization of prepared samples is very important. We have used XRD for structure analysis, SEM and TEM for estimation of particle size, AFM for measure for the measure of roughness of surface.

1.4.2 Classes of Multiferroics

The microscopic origin of magnetism is basically the same in all magnets; it is the presence of localized electrons, mostly in the partially filled d of f shells of transition metal or rare earth ions, which have corresponding localized spin, or magnetic moment. Exchange interactions between localized moments lead to magnetic order. However the situation is different in case of ferroelectrics. There are several different microscopic origins of ferroelectricity and accordingly one can have different types of multiferroics. Generally the multiferroics are categorized in two groups: (i) type I multiferroics and (ii) type II multiferroics, on the basis of the origin of ferroelectricity in them [20].

1.4.3. Type I Multiferroics

This group of multiferroics contains those Pervoskite in which Ferroelectricity and ferromagnetism have different sources (cations at A-site and B-site respectively). These materials show weak magneto electric coupling. In these materials, ferroelectricity typically appears at higher temperatures than magnetism and they exhibit large spontaneous polarization. Examples are $BiFeO_3$ (T_c^{FE} ~ 1110 K, T_N ~ 643 K, P ~ 90 μC/cm^2), $YMnO_3$ (T_c^{FE} ~ 914 K, T_N ~ 76 K, P ~ 6 μC/cm^2). These materials have been extensively studied since 1960's. However, major challenge in these materials is to enhance the values of magneto electric coupling coefficient. Type I multiferroics are further classified in many subclasses on the basis of origin of Ferroelectricity.

(i) *Ferroelectricity due to shifting of B-cation*

(ii) *Ferroelectricity due to lone pairs*

(iii) *Ferroelectricity due to charge ordering*

(iv) *"Geometric" Ferroelectricity*

1.4.4. Type II Multiferroics (Magnetic Multiferroics)

The materials in which the Ferroelectricity is originated from magnetism and exhibit strong magneto electric coupling. However the polarization in these materials is usually much smaller (10^{-2} μC/cm^2). These multiferroics are recently discovered. $TbMnO_3$ and $TbMn_2O_5$ are typical examples of these materials [13, 21]. Kimura *et al.* [13] demonstrate strong influence of magnetic field on electric polarization. In $TbMnO_3$, the polarization rotates (or "flops") by 90 degrees when a critical field is applied in a

certain direction [18]. Influence of magnetic field is even stronger in case of $TbMn_2O_5$ [21]. The polarization changes sign with magnetic field. With the discovery of these materials, a number of other type-II multiferroics with strong magneto electric coupling have been discovered and studied. On the basis of mechanism of multiferroic behavior, one can divide type-II multiferroics in two categories.

(i) *Spiral Type-II Multiferroics*

(ii) *Type-II Multiferroics with Collinear Magnetic Structures*

1.4.5. Multiferroic Composites:

An alternative approach to get the enhanced magneto electric coupling is to introduce indirect coupling, via strain [22], between two materials such as a ferromagnetic and a ferroelectric. Strain coupling requires intimate contact between a piezomagnetic (or magnetostrictive) and a piezoelectric (or electrostrictive) material. This can be achieved in the form of composites [22], laminates [23-25] or epitaxial multilayer's. The coupling constant depends on the frequency of the *ac* magnetic field and such multiferroic structures are useful in technical applications, *e.g.*, microwave frequency transducers.

1.4.6. Applications of Multiferroics

Most of the research in multiferroics has been curiosity driven basic research, but there are a number of ideas for device applications based on multiferroic materials. One of the more popular ideas is that multiferroic bits may be used to store information in the magnetization *M* and the polarization *P*. The feasibility of such a 4 stage memory (two magnetic M↑↓ and two ferroelectric P↑↓) has been demonstrated recently [16, 26]. Such a memory does not require the coupling between Ferroelectricity and magnetism; a cross coupling would be even disastrous. If magneto electric coupling is present, device applications could be realized where information is written magnetically, but stored in the electric polarization, leading to non-volatile memory

CHAPTER 2

CERAMICS TECHNOLOGIES AT A GLANCE (BULK AND THIN FILMS)

All compositions in bulk presented in this thesis were synthesized by conventional ceramic technique. The specimens for characterization and the ceramic target prepared for preparation of thin films by Pulse Laser Deposition (PLD) technique were made by compacting the reacted powder, followed by sintering. In this chapter, the ceramic technology employed for the preparation of ceramic bulk and thin films are discussed. Sol gel technique has been utilized here for better tailoring of compositions for the preparation of thin films.

2.1. Solid State Route

A number of techniques are normally used to synthesise ceramic materials. Solid state route is one of them which is conventional and simplest way to prepare ceramic material compositions of required shapes and electrical properties with cost effectiveness. In this methodology of preparation, the metal oxides/carbonates of analytical grade (AR grade) are taken as starting materials. These oxide materials are weighed in desired stoichiometric ratio and ball milled (dry or wet, depending upon milling techniques) to get fine particle size (typically between 1 to 10 μm) [26]. The metal oxides normally do not react at room temperature. In order to facilitate the reaction to occur, they are heated to higher temperature. The powders are then subjected to temperatures (800^{o}C or so) for calcinations. Calcination causes the constituents to interact by inter diffusion of their ions and resulting in a homogeneous compound. After calcination, the powders are ball milled again for better homogeneity. Further it is compacted to the desired shape by several compaction techniques like uniaxial pressing, iso-static pressing, hot pressing, hot iso-static pressing etc. The final stage of preparation of ceramics by solid state route ends with sintering which provides densification (>95 %) depending upon the optimized processing parameters, pressing technique and programmed sintering. After sintering the compacted and sintered ceramics can be cut to desired shapes, lapped, polished and electroded before electrical characterization.

Perovskite ferroelectrics form an important class of electroceramic materials and are widely used in a number of electronic applications. Properties of these ceramics are controlled predominantly by compositions. But at the same time these properties are affected by the grain size, porosity and method of fabrication. The main objective for the fabrication of electroceramics is to prepare materials with specific electrical properties. A solid solution is a single phase material of two or more compounds whose characteristics are changed but structure is retained. Usually polycrystalline materials are prepared by this solid state route and hence they are termed as conventional route also. Amongst the non conventional methods, hydrothermal synthesis, spray drying techniques, wet chemical methods are commonly used for preparation of ceramic materials.

2.2. Sol-gel Technique

The sol-gel thin film deposition technique has attracted the reseracher's maximum attention for a variety of materials [27]. Budd et al [28] used this technique for the deposition of ferroelectric thin films such as lead titanate ($PbTiO_3$), lead zirconate ($PbZrO_3$), lead zirconate titanate {$Pb(Zr,Ti)O_3$} and lanthanum modified lead zirconate titanate {$(Pb,La)(Zr,Ti)O_3$} [28]. Literature survey on ferroelectric thin films preparation shows that the sol-gel technique continues to be the preferred method as compared to other physical and chemical methods [29-31]. High quality ferroelectric thin films of different compositions are being obtained by sol-gel process [32-39]. Unlike physical deposition methods, the sol-gel route does not require very sophisticated and expensive equipment. Further, the compositions of even complex type of perovskite ceramics also can be controlled prepared using this technique. Thus the properties of the ceramics can be easily tailored using this sol gel thin film deposition technique.

A definition of the sol-gel process has been proposed and introduced by D.L. Segal i.e. "Sol-gel is the process of production of inorganic oxides either from colloidal dispersion or from metal alkoxides" [40]. However, the sol-gel technique includes the hybrid organic-inorganic materials also [41]. The definition of Segal hold good only for the ferroelectric thin films, where the alkoxides are the starting reagents which has been used for the present research work. Alkoxides are the compounds which are generalized by a chemical formula $M(OR)_n$. They are obtained from direct or indirect reactions between a metal 'M' and an alcohol 'ROH' (R : C_2H_5, C_3H_7, C_4H_9 etc.). First of all the

precursor solution (sol) is made usually by mixing the alkoxide with an appropriate solvent. There are mainly two processes which determine the structure and characteristics of particles in a sol. The first one is hydrolysis:

$$M(OR)_n + H_2O \rightarrow M(OR)_{n-1}(OH) + ROH \quad (2.1)$$

Since metal alkoxides are very reactive due to the presence of highly electronegative –OR groups (alkoxide group), the kinetic of reaction (2.1) is sensitive to ambient conditions, and sometimes the sol preparation requires an inert atmosphere with controlled humidity (i.e in N_2, or in a glove box). The second process involves the formation of M-O-M bonds by oxolation reactions [42, 43].

$$2M(OR)_{n-1}(OH) \rightarrow M_2O(OR)_{2n-2} + H_2O \quad (2.2)$$

or,

$$M(OR)_n + M(OR)_{n-1}(OH) \rightarrow M_2O(OR)_{2n-2} + ROH \quad (2.3)$$

A number of methods regarding solution preparation can be thought of based on the starting reagent used and the chemical reactions involved in alkoxide modification. The first one utilizes $C_3H_8O_2$ (2-methoxyethanol) as solvent. In this case, the alkoxide modification occurs in the course of an alkoxy exchange reaction:

$$M(OR)_n + nR'OH \rightarrow M(OR')_n + nROH \quad (2.4)$$

here, -OR' is the methoxyethoxy group. The resultant methoxyethoxide $M(OR')_n$ is usually more stable and less sensitive to water.

The “hybrid” or “chelate” process uses other reagents for alkoxide modification by the chelating reaction:

$$M(OR)_n + xCH_3COOH \rightarrow M(OR)_{n-x}(OOCCH_3)_X + xROH \quad (2.5)$$

Though as a chelating agent acetylacetone or acetic acid [44 - 46] is usually used, 2-methoxyethanol can be preferred as a final solvent and agent controlling concentration and rheology of the solution. Further growth of sol species, which are oligometric in nature, leads to the gelation of the sol following process similar to (2.2) or (2.3). This is the next step of the sol-gel process. Further a gel is a porous 3-dimensionally interconnected pseudo-solid that expands throughout a liquid, and is limited only by the size of the container. In the case of sol-gel processing of thin films, spin-coating, dip-coating or spray-pyrolysis routes are usually utilized to deposit thin layers. The gel should be dried at moderate temperatures (~ 80^{o}C) to evaporate the solvent. The final

product is annealed at high temperature (less than 650°C) in order to complete phase transformation.

2.3. Pulse Laser Deposition (PLD)

Among the present thin film deposition techniques, pulsed laser deposition (PLD) technique has emerged as one of the best techniques to grow a stoichiometric film from the stoichiometric target. A comparison has been reported and shown in the Table 2.1 showing the performance of the other deposition techniques in terms of the growth rate, stoichiometry, epitaxy and limitations [22]. Pulsed Laser Deposition (PLD) or Laser induced vaporization (laser ablation) is a film deposition technique in which a plume of ionized and ejected material is produced by high intensity laser irradiation of a solid target. Most commonly, UV excimer lasers are being employed for this purpose and the wavelength of the radiation is tuned by the lasing gas composition, such as ArF (193 nm), KrF (248 nm), KrCl (222 nm), XeF (351 nm) and XeCl (308 nm). KrF (248 nm) has been most dominently employed due to the high energy laser pulse output. KrF is the highest gain system for electrically discharged pumped excimer lasers and is a popular choice among the PLD community. This technique is currently being employed for the insitu growth of device quality ferroelectric PZT thin films [23-24]. Pluse to pulse variations are of the order of 5%, while the pulse durations can be 10-25 ns and repetition rates upto 500 Hz.. However, for the present study, an excimer laser with 25 ns pulse width (FWHM) and 10 Hz repetition rate was employed. PLD technique is state of the art thin film deposition technique for transferring or depositing the target material directly to the substrate. surface and placed few cm's distant apart inside a vacuum chamber. The chamber consists of a target holder with an arrangement for its rotation and a substrate holder with heating arrangement for in-situ cystallisation. In order to change the target-substrate distance, substrate holder can be moved. A high power laser is used as an external energy source to vaporize materials which can absorb energy and get deposited on the substrate. For focusing the laser beam and its manipulation, UV compatible optics is used. In this technique, the source of energy i.e. laser is not affected by deposition environment as the source is externally placed and is independent of deposition chamber. Film growth can be carried out in a reactive environment also containing any kind of gas

with or without plasma excitation. In the present study, only oxygen gas has been used as reactive gas. It can also be operated in conjunction with other types of evaporation sources in a hybrid approach. PLD is so versatile that with the choice of an appropriate laser, it can be used to grow thin films of almost any kind of material. The use of short laser pulses offers other advantages such as congruent ablation that allows PLD to preserve stoichiometry during mass transfer from the target to the substrate. During laser ablation there are mainly three interaction regions:-

(a) Interaction of laser beam with target,

(b) Interaction of the laser beam with evaporated materials, and

(c) Adiabatic plasma expansion and deposition of thin films.

The plume formed during ablation of the material is always perpendicular to target surface irrespective of the angle of incidence of laser beam and the generated plasma plume is composed of neutrals, ionised atomic and mostly molecular species. This technique has been popularly employed for the successful deposition of high T_c superconductors. The laser ablation offers several advantages. They are:

(a) Composition of the film deposited are similar to that of target, even for complex multi-component systems,

(b) Deposition at relatively high oxygen partial pressures is possible,

(c) Low crystallization temperatures because of the high excitation energy of the photo fragments in the laser produced plasma,

(d) Higher deposition rates and

(e) Materials with high melting temperatures can be deposited.

Thin films of oxides deposited by laser ablation and other ceramics have generated much attention during 1980s. The success of high temperature superconductor film growth provided the focus needed to accelerate the development of the field. The ability to preserve the stoichiometry of a multicomponent system to oxygenate films in situ by reactive deposition and to easily evaporate just about any material have finally merged. The latest trends include even the Buckminster fullerence (i.e. C_{60}) in addition to deposition of ferroelectric and other types of thin films like CdTe, CdS, metal films etc. The detailed list of the ablated materials has been already reported [47-50].

CHAPTER 3

EXPERIMENTAL METHODS

In this chapter we will discuss the theory and concepts behind the analytical techniques that are used to analyze our data. We have used some standard software's/methods like Rietveld refinement (for analyzing the XRD data and Neutron diffraction data), Z-view for impedance profile fitting, Maxwell-Wagner Model and Joncscher's universal law for ac conductivity. These models and methods are discussed as follows.

3.1. Sol-Gel Technique: Spin Coating Method

Spin coating has been used for the deposition of thin films. This process involves a small amount of solution onto the centre of a substrate and then spinning the substrate putting at high speed. Final film thickness and other properties will depend on the nature of the solution (viscosity, drying rate, surface tension etc.) and the parameters chosen for the spin process such as rpm and spin time. The spin coating process involves four stages shown in the Figure 3.1. The deposition, spin up, and spin off stages occur sequentially while the evaporation stage occurs throughout the process, becoming the primary means of thinning near the end. The Figure 3.1 shows the stages involved in spin coating process. The important factors such as final rotational speed, acceleration, and solvent evaporation rate contribute how the properties of the coated films are defined. One of the most important factors in the spin coating is repeatability. Slight variations in the parameters that define the spin process can result in drastic variations in the coated film. The deposition process involves the dispense of an excessive amount of fluid onto a stationary or slowly spinning substrate. The fluid is deposited through a nozzle at the centre of the substrate. In Figure 3.2 shows the spin coater apparatus. An excessive amount of fluid is used to prevent the coating discontinuities caused by a fluid front drying prior to it reaching the wafer edge. In the spin up stage, the substrate is accelerated to the final spin speed. As rotational forces are transferred upward through the fluid, a wave front forms and flows to the substrate edge by centrifugal force, leaving a fairly uniform layer of solution during the spin off stage the excessive solvent is flung off the substrate surface as it rotates at speeds between 2000 and 5000 rpm. The fluid is being

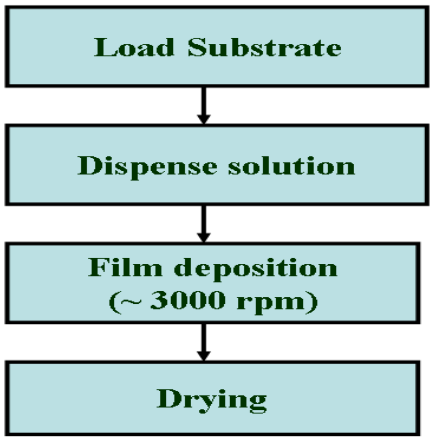

Fig. 3.1. Spin coating process

Fig.3.2: Sol-Gel Method Spin Coater

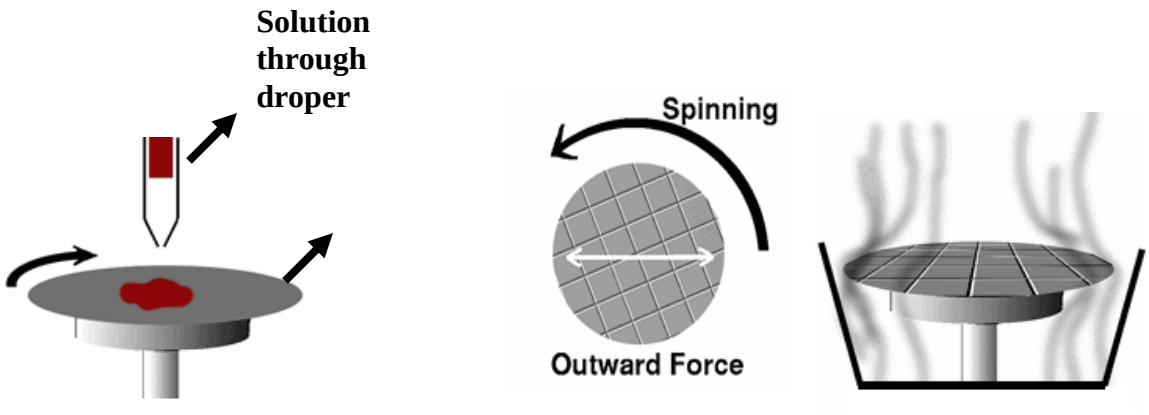

Fig. 3.3 Spin coater parts

thinned primarily by centrifugal forces until enough solvent has been removed to increase the viscosity to a level where flow ceases. Throughout the spin coating process, evaporation becomes the primary method of film thinning once fluid flow ceases. Evaporation is the complex process by which a portion of the excess solvent is absorbed into atmosphere.

Spin coating is a technique used to apply uniform film to flat substrate. An excess amount of solution in place on the substrate which is kept on a rotating platform (whose rotation can be controlled manually or by computer that depend on the type spin coater one is using) which is then rotated at high speed in order to spread the fluid by centrifugal force. The platform is such that there is small hole at the center of platform which is connected to vacuum pump. When a flat substrate is kept on platform substrate, it close the small hole and then vacuum is created inside, so that substrate stick to the platform and when platform rotates only solution could move on the substrate. A machine used for used for spin coating is called a spin coater or simple spinner. Rotation is continued while the fluid spins off the edges of the substrate, unit the desire thickness of the film is achieved. The higher the angular speed of spinning, the thinner the film. The thickness also depends on the concentration of the solution and solvent.

Spin coating is widely used in micro fabrication, where it can be create thin film with thicknesses below 10 nm. It is used intensively in photography, to deposit layer of the photoresist about 1 micrometer thick. Photoresist is typically spun at 20 to 80 revolutions per second for 30to 60 second. All compositions in thin film presented in this thesis were synthesized by conventional ceramic technique. The specimens for characterization and the ceramic target prepared for preparation of thin films by Pulsed Laser Deposition (PLD) technique followed by annealing. In this chapter, the ceramic technology employed for the preparation of ceramic bulk and thin films are discussed. Sol gel technique has been utilized here for better tailoring of compositions for the preparation of thin films.

The usefulness of each deposition technique depends on their specific capabilities and limitations. Deposition techniques for BF/PZT thin films include:

- Pulsed laser deposition
- Sputtering deposition
- Chemical Vapor Deposition
- Spray Pyrolysis
- Sol Gel
- Microwave Irradiation
- Wet Oxidation

3.1.1. Sol-Gel Technique

The sol-gel thin film deposition technique has attracted the reseracher's maximum attention for a variety of materials [51]. Budd et al [52] used this technique for the deposition of ferroelectric thin films such as bismuth ferrite ($BiFeO_3$) lead titanate ($PbTiO_3$), lead zirconate ($PbZrO_3$), lead zirconate titanate {$Pb(Zr,Ti)O_3$} and lanthanum modified lead zirconate titanate {$(Pb,La)(Zr,Ti)O_3$} [52]. Literature survey on ferroelectric thin films preparation shows that the sol-gel technique continues to be the preferred method as compared to other physical and chemical methods [53-56]. High quality ferroelectric thin films of different compositions are being obtained by sol-gel process.Figure 3.4 describes the Sol-Gel process. Unlike physical deposition methods, the sol-gel route does not require very sophisticated and expensive equipment. Further, the compositions of even complex type of perovskite ceramics also can be controlled

prepared using this technique. Thus the properties of the ceramics can be easily tailored using this sol gel thin film deposition technique. A definition of the sol-gel process has been proposed and introduced by D.L. Segal i.e. *"Sol-gel is the process of production of inorganic oxides either from colloidal dispersion or from metal alkoxides"* [57]. However, the sol-gel technique includes the hybrid organic-inorganic materials also [58]. The definition of Segal hold good only for the ferroelectric thin films, where the alkoxides are the starting reagents which has been used for the present research work. Alkoxides are the compounds which are generalized by a chemical formula $M(OR)_n$. They are obtained from direct or indirect reactions between a metal 'M' and an alcohol 'ROH' (R: C_2H_5, C_3H_7, C_4H_9 etc.). First of all the precursor solution (sol) is made usually by mixing the alkoxide with an appropriate solvent.

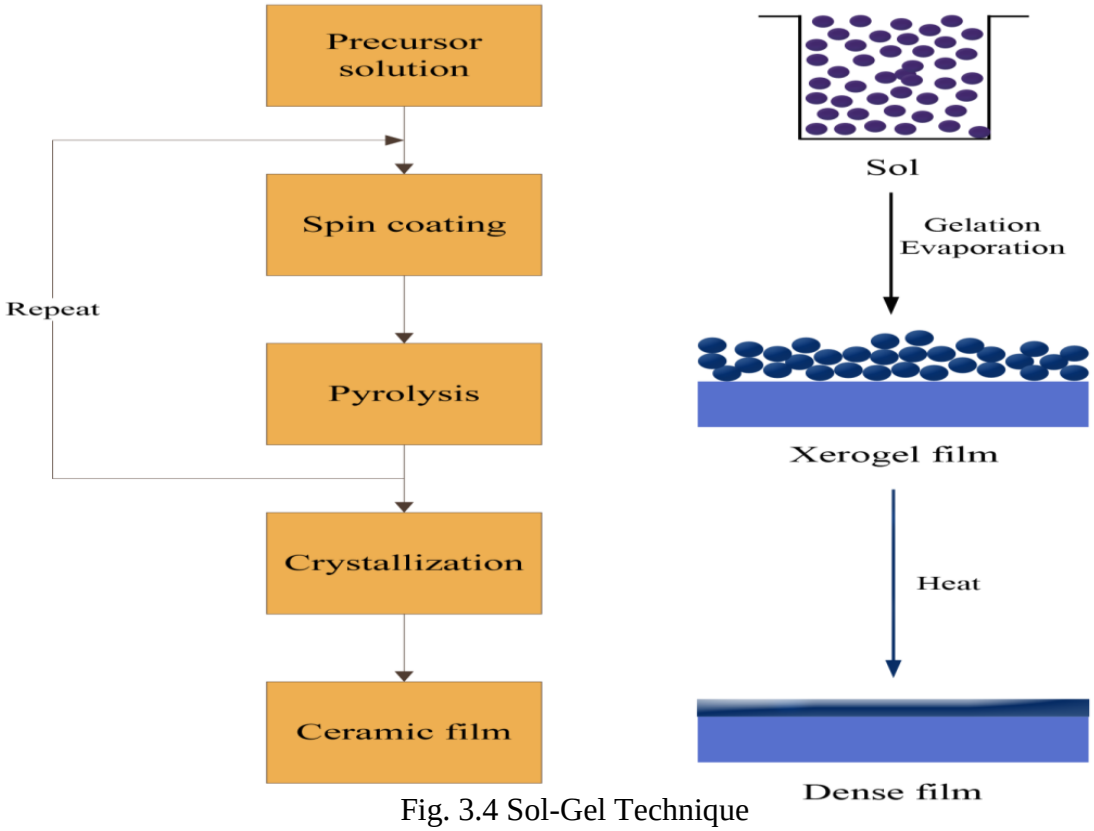

Fig. 3.4 Sol-Gel Technique

$$M(OR)_n + H_2O \rightarrow M(OR)_{n-1}(OH) + ROH$$

Since metal alkoxides are very reactive due to the presence of highly electronegative –OR groups (alkoxide group), the kinetic of reaction (3.1) is sensitive to ambient conditions, and sometimes the sol preparation requires an inert atmosphere with controlled humidity (i.e in N_2, or in a glove box). The second process involves the formation of M-O-M bonds by oxolation reactions :

$$2M(OR)_{n-1}(OH) \rightarrow M_2O(OR)_{2n-2} + H_2O \qquad (3.2)$$

or,

$$M(OR)_n + M(OR)_{n-1}(OH) \rightarrow M_2O(OR)_{2n-2} + ROH \qquad (3.3)$$

A number of methods regarding solution preparation can be thought of based on the starting reagent used and the chemical reactions involved in alkoxide modification. The first one utilizes $C_3H_8O_2$ (2-methoxyethanol) as solvent. In this case, the alkoxide modification occurs in the course of an alkoxy exchange reaction:

$$M(OR)_n + nR'OH \rightarrow M(OR')_n + nROH \qquad (3.4)$$

here, -OR' is the methoxyethoxy group. The resultant methoxyethoxide $M(OR')_n$ is usually more stable and less sensitive to water.

The “hybrid” or “chelate” process uses other reagents for alkoxide modification by the chelating reaction:

$$M(OR)_n + xCH_3COOH \rightarrow M(OR)_{n-x}(OOCCH_3)_X + xROH \qquad (3.5)$$

Though as a chelating agent acetylacetone or acetic acid [59-62] is usually used, 2-methoxyethanol can be preferred as a final solvent and agent controlling concentration and rheology of the solution. Further growth of sol species, which are oligometric in nature, leads to the gelation of the sol following process similar to (3.2) or (3.3). This is the next step of the sol-gel process. Further a gel is a porous 3-dimensionally interconnected pseudo-solid that expands throughout a liquid, and is limited only by the size of the container. In the case of sol-gel processing of thin films, spin-coating, dip-coating or spray-pyrolysis routes are usually utilized to deposit thin layers. The gel should be dried at moderate temperatures (~ 80^oC) to evaporate the solvent. The final product is annealed at high temperature (less than 650°C) in order to complete phase transformation.

Sol-Gel method has many advantages over other hand. They are listed as following.

1) The Sol-Gel method is very cheap and law temperature technique that allows for the fine control of the product's chemical composition.

2) The Sol-Gel is used for preparation of powder as well as very thin film.

3) Sol-Gel derived materials have divers applications in optics, energy, space, biosensor, medicine, reactive material and separation (e.g. chromatography) technology.

4) In Sol-Gel method the product obtained is very highly pure and homogenous.

3.1.2. Precursor Routes and Deposition for Lead Zirconium Titanium Oxide {Pb ($Zr_{.52}Ti_{.48}$) O3}:

Though there are many precursors for preparation of PZT, The flow diagram to synthesize the precursor solution for the PZT thin films is given in Fig. 3.5. Lead acetate trihydrate and zirconium nitrate pentahydrate are initially dissolved in 2-methoxyethnaol, and refuxed for 1 h at 100 ^{o}C. During the refux, appropriate quantity of acetylacetone is added to the solution to stabilize the solution. The associated water is removed during a period of distillation at 125 ^{o}C. After cooling to room temperature, the required quantity of titanium n-butoxide is added to the solution and mixed in the flask at 80 ^{o}C. Then the solution is refuxed for 1 h, and subsequently distilled to remove the byproduct. The solution is stable and no crystallite forms for several months. For good quality of film to be deposited substrate should be cleaned properly. The concentration of the "solution can be adjusted to 0.4Mby adding or distilling appropriate quantity of solvent. The whole process of the preparation of the precursor solution is performed in an ambient atmosphere. Before spin-coated on the substrates, the solution is "filtrated with a 0.2 um syringe "filter to avoid particulate contamination. The thermal treating process for the samples is completed in a rapid thermal annealing (RTA) furnace. The heating chamber is composed of two banks of halogen lamps placed above and below a quartz box. The coating solution for the PZT "films are deposited onto Pt/Ti/SiO2/Si substrates by spin-coating. A layer by- layer annealing method is carried out in the procedure of heat treatment. Each layer of the wet "film is dried at 1803C for 300 s and then directly annealed in the RTA furnace at a higher temperature for 180 s. This step is repeated six times to obtain the desired thickness of the "films. The annealing temperatures varied from 450 to 600 ^{o}C. The process of the heat treatment is completed in air atmosphere.

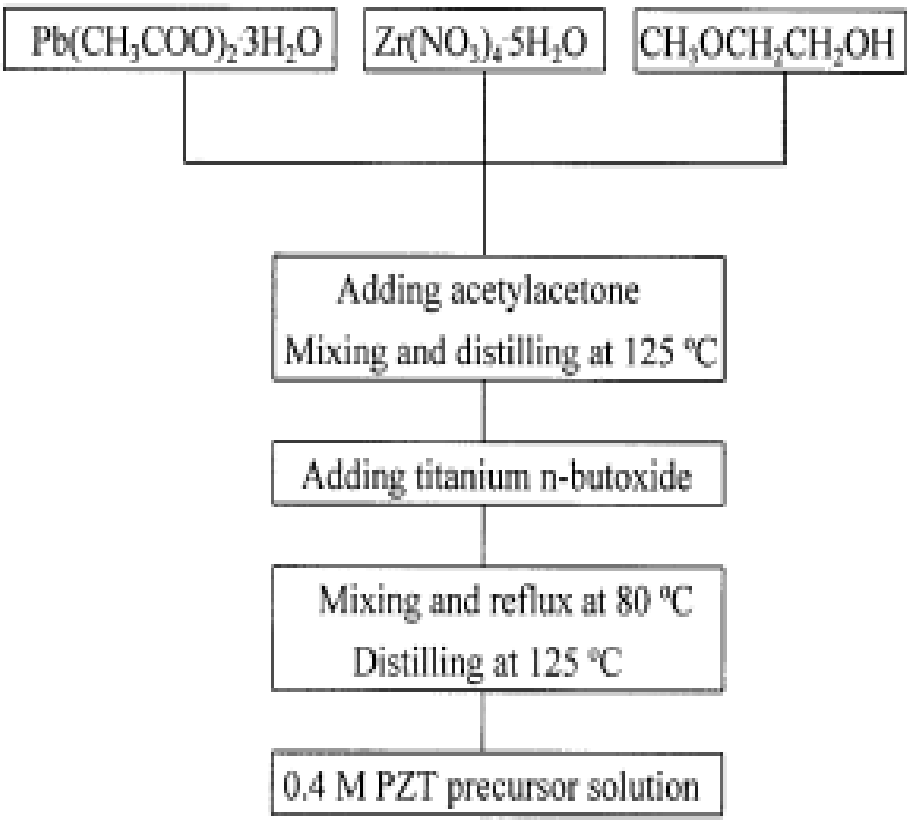

Fig. 3.5 Flow chart for PZT sol preparation

3.1.3. Precursor Routes and Deposition for Bismuth Ferrite-Lead Zirconate Titanate ($BiFeO_3$-$PbZrTiO_3$):

$PbZrTiO_3$ precursor solutions with excess Pb acetate 10 mol% were prepared using the sol-gel method from Pb acetate tryhydrate [Pb $(CH3CO_2)_2.3H_2O$], Zirconium nitrate trihydrade [Zr $(NO_3)_3$].$3H_2O$, and Titanium Butoxide} as the starting materials, and 2-methoxyethanol ($CH_3OCH_2CH_2OH$) as the solvent. BiFeO3 precursor solutions were prepared using the sol-gel method with Bi nitrate pentahydrate [Bi $(NO_3)_3.5H_2O$] and Fe(III) nitrate nonahydrate [$Fe(NO_3)_39H_2O$] as the starting materials, and 2-methoxyethanol and acetic acid [CH_3COOH] as the solvent. The PZT precursor solution was passed through a syringe filter and spin-coated on the Pt(200 m)/Ti(20 nm)/SiO2/p-Si(100) substrates using a spinner operated at 6000 rpm for 60 sec to form the first layer. These $PbZrTiO_3$ films were dried at 300 ^oC for 30 min to remove the organic materials,

and sintered at 600 ^{o}C for 30 min to crystallize them into the perovskite structure. The BFO precursor solution was then spin-coated and dried/sintered on the PZT films to form the second layer under sintering conditions of 600 ^{o}C for 10 min. This procedure was repeated several times, and the $BiFeO_3$-$PbZrTiO_3$ heterolayered thin films were fabricated. The crystallinity of the $BiFeO_3$/$PbZrTiO_3$ films was analyzed using X-ray diffraction (XRD), and the surface, cross-sectional morphologies and thickness of the films were examined by scanning electron microscopy (SEM). For electrical measurements, Pt thin films were dc sputter-deposited on the $BiFeO_3$-$PbZrTiO_3$ thin films as the top electrode with diameter of a 250 nm.

3.2. Characterization Technique

3.2.1. X-ray Diffraction (XRD):

X-ray diffraction (XRD) is a rapid analytical technique used for phase identification of a crystalline material, measurement of sample purity and can provide information of unit cell dimensions. X-ray diffraction is based on constructive interference of monochromatic X-rays and a crystalline sample. These X-rays are generated by a cathode ray tube, filtered to produce monochromatic radiation, collimated to concentrate, and directed toward the sample. The interaction of the incident rays with the sample produces constructive interference (and a diffracted ray) when conditions satisfy Bragg's Law ($n\lambda=2d \sin\theta$) as shown in Figure 3.6.

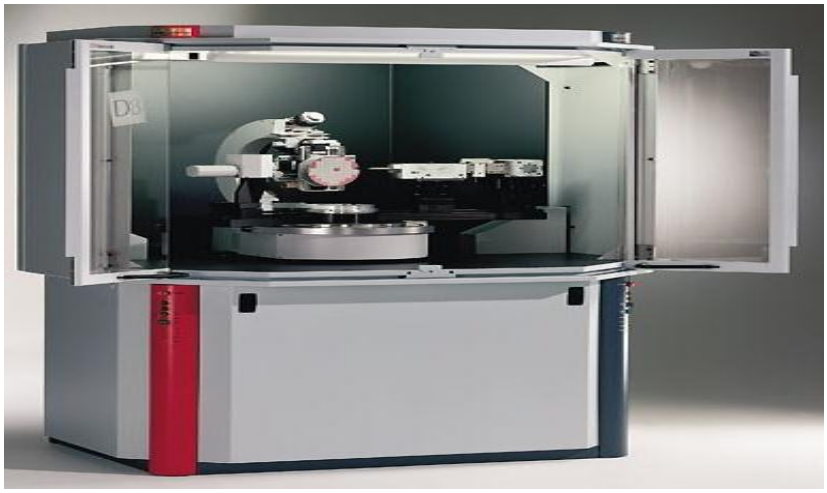

Fig.3.6. Schematics of X-ray diffraction

This Bragg's law relates the wavelength of electromagnetic radiation to the diffraction angle and the lattice spacing in a crystalline sample. These diffracted X-rays are then detected, processed and counted. By scanning the sample through a range of 2θ angles, all possible diffraction directions of the lattice should be attained due to the random orientation of the powdered material. Conversion of the diffraction peaks to d-spacing allows identification of the mineral because each mineral has a set of unique d-spacing. Typically, this is achieved by comparison of d-spacing with standard reference patterns.

A typical X-ray diffractometer as shown in Figure 3.6 consists of three basic components: An X-ray tube, a sample holder, and an X-ray detector. X-rays are generated in a cathode ray tube by heating a filament to produce electrons, accelerating the electrons toward a target by applying a voltage, and bombarding the target material with electrons. When electrons have sufficient energy to dislodge inner shell electrons of the target material, characteristic X-ray spectra are produced. These spectra consist of several components, the most common being K_α and K_β. K_α consists, in part, of $K_{\alpha1}$ and $K_{\alpha2}$. $K_{\alpha1}$ has a slightly shorter wavelength and twice the intensity as $K_{\alpha2}$. The specific wavelengths are characteristic of the target material (Cu, Fe, Mo, Cr). Filtering, by foils or crystal monochromators, is required to produce monochromatic X-rays needed for diffraction. $K_{\alpha1}$ and $K_{\alpha2}$ are sufficiently close in wavelength such that a weighted average of the two is used.

Copper is the most common target material for single-crystal diffraction, with CuK_α radiation = 1.541 Å. These X-rays are collimated and directed onto the sample. The collimation is performed using cones or collimators (multi-leaf collimator or iris diaphragms) that are attached directly in front of X-ray tube. As the sample and detector are rotated, the intensity of the reflected X-rays is recorded. When the geometry of the incident X-rays impinging the sample satisfies the Bragg equation, constructive interference occurs and a peak in intensity occurs. A detector records and processes this X-ray signal and converts the signal to a count rate which is then output to a device such as a printer or computer monitor.

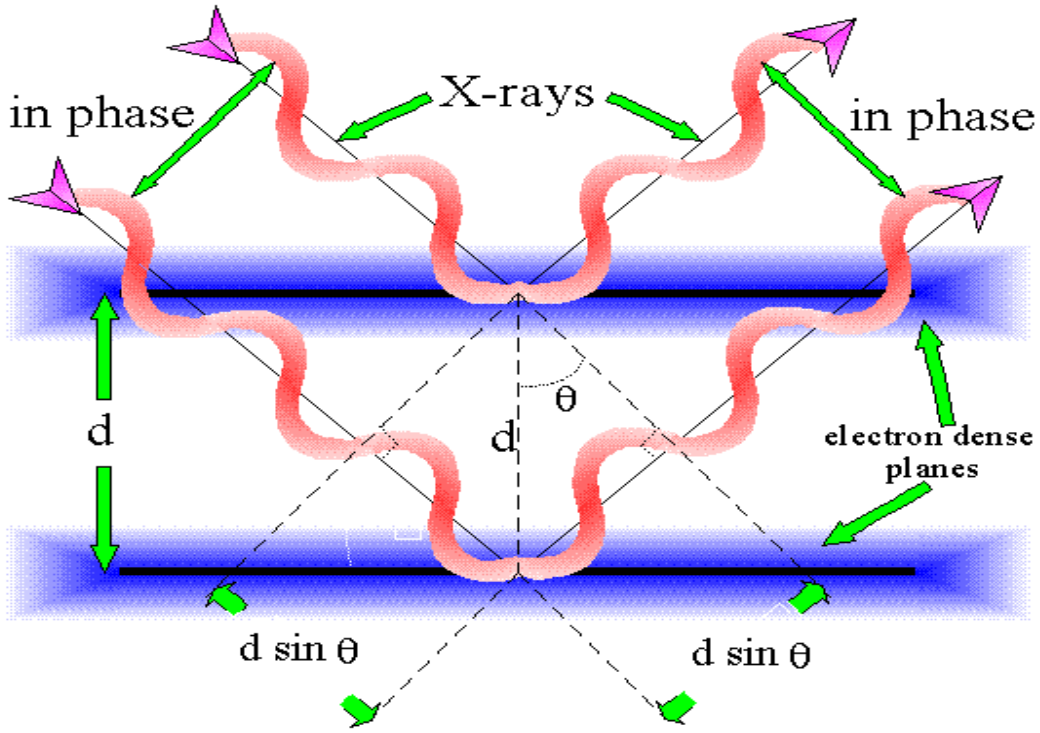

Fig 3.7.Basic principle involved in diffraction of X- ray beam from assembly of lattice atoms)

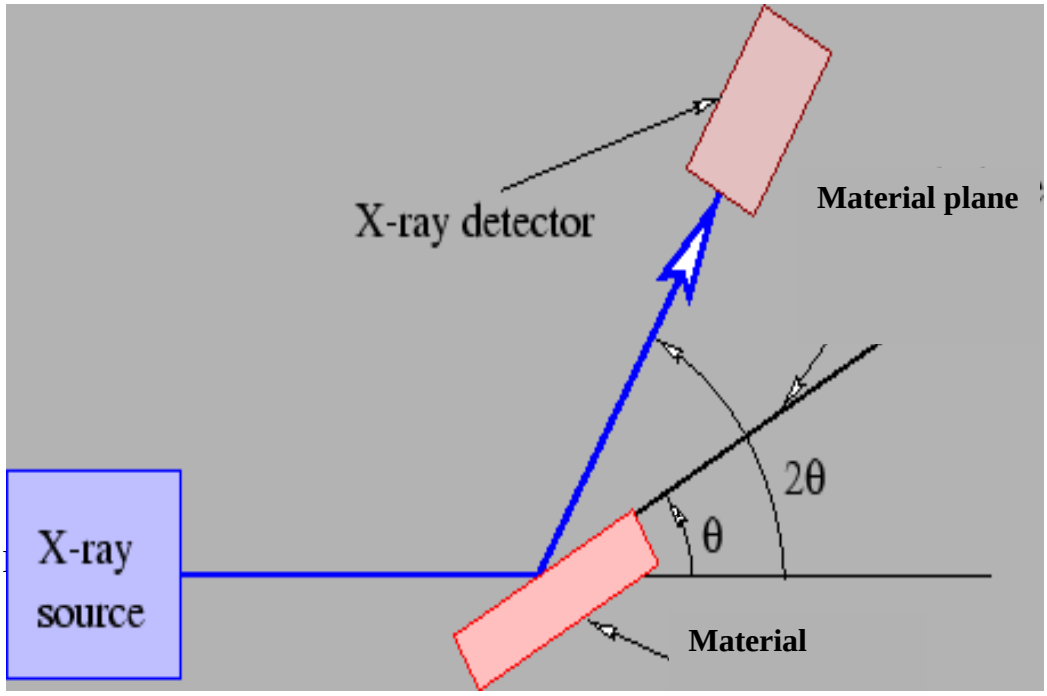

(also known as crystallites) is not uniform and cannot be singled out to be characterized in the same way than single crystals. In a crystal, there are several families of planes with different orientations however interplanar distance among them is constant. In the case of a polycrystalline sample, the variable orientation and size of the crystallites will produce the number of families of planes contributing to one Bragg peak as well as the interplanar distances to be different than the single crystal case. In polycrystalline diffraction it is preferable to have a sample with a smooth plane surface, with crystallites randomly distributed. Only crystallites having reflecting planes (*hkl*) parallel to the specimen surface will contribute to the reflected intensities.

The geometry of an X-ray diffractometer is such that the sample rotates in the path of the collimated X-ray beam at an angle θ while the X-ray detector is mounted on an arm to collect the diffracted X-rays and rotates at an angle of 2θ. The instrument used to maintain the angle and rotate the sample is termed a goniometer.

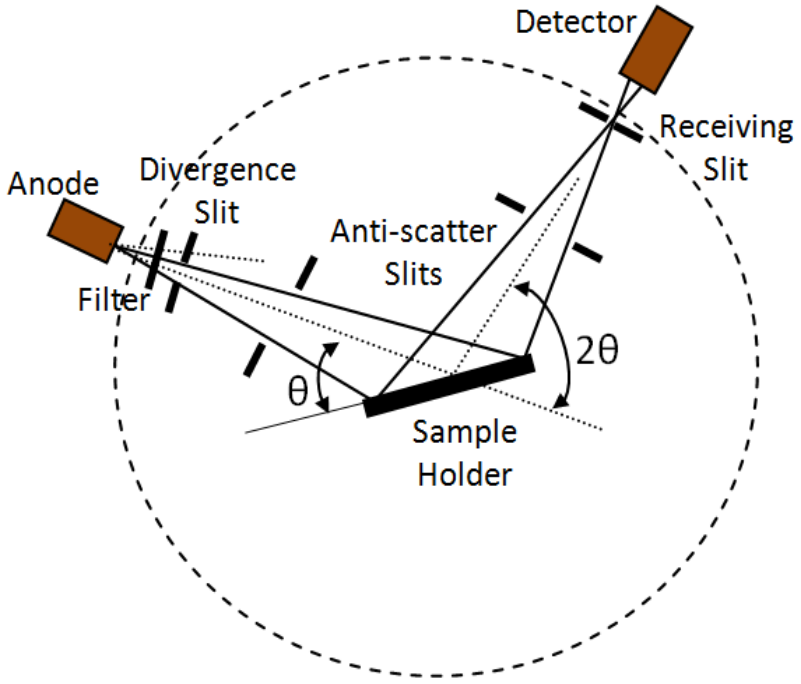

Fig.3.9 Schematic of the X-rays experimental setup.

For a hexagonal system the value of the lattice parameters ‘a’ and ‘c’ can be calculated using the relation

$$\frac{1}{d_{hkl}^2} = \left[\frac{4}{3} \cdot \frac{h^2 + hk + l^2}{a^2} + \frac{l^2}{c^2} \right]$$

The lattice parameters of our samples were calculated by using [hkl] values of the diffraction peaks situated at higher 2θ values for better accuracy.

3.2.2. Scanning electron Microscope (SEM)

The scanning electron microscope (SEM) is a type of electron microscope that images the sample surface by scanning it with a high-energy beam of electrons in a raster scan pattern. The scanning electron microscopy is used for inspecting topographs of the specimen at very high magnification more than 300,000X. In this process the electrons interact with the atoms that make up the sample producing signals that contain information about the sample's surface topography. The types of signals produced by an SEM include secondary electrons, back scattered electrons (BSE), characteristic x-rays, light (cathode luminescence), specimen current and transmitted electrons. These types of signals require specialized detectors for their detection that are not usually all present on a single machine. The signals result from interactions of beam with atoms at or near the surface of the sample. The schematic diagram of the arrangement of different lenses is shown in fig. 2.5. During SEM inspection, a beam of the electron is focused on a spot volume of the specimen, resulting in transfer of energy on the spot these bombarding electron also called the primary electrons, removes the secondary electron from the specimen itself. The intensity and spot size of the beam can be adjusted by varying the current in these lenses. The beam finally passes through an objective lens that focuses the beam to a very small spot on the sample. Scanning coils scan the electron beam falling on the sample in the controlled way. The scan coils are energized (by the voltage produced by the scan generator) and create a magnetic field, which deflect the beam back and forth in a controlled manner.


Interpupillary adjustment
Ocular (eyepiece)
Body
Nosepiece
Objective lens (4)
Mechanical stage
Substage condenser
Aperture diaphragm control
Base with light source
Field diaphragm lever
Light intensity control
Arm
Coarse focus adjustment knob
Fine focus adjustment knob
Stage adjustment knobs
Leica
ATC 2000

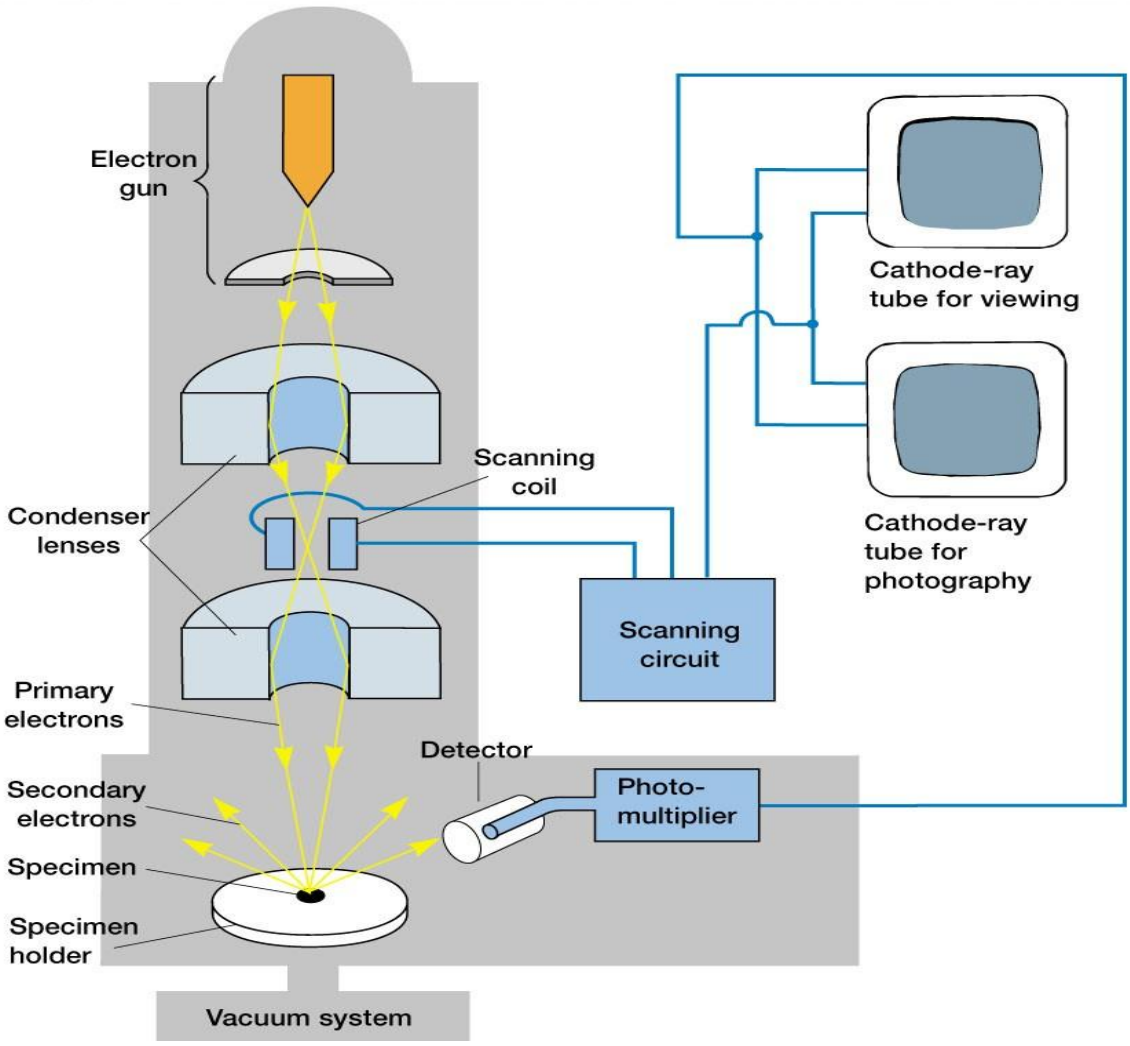

Fig 3.10. Diagram of Scanning Electron Microscope.

The electron beam, which strikes the specimen, produces the secondary electrons from the specimen. The secondary electrons emitted from the surface are highly surface specific and those only emitted at a depth of 20 Aº from the surface are able to reach the detector. Secondary detector produces a voltage pulse, which is proportion to the intensity of the secondary electron emitted from the sample surface. The voltage signal is amplified and applied to the grid of the cathode ray tube that causes the intensity of the luminescent spot on the phosphor screen to the change. The image consists of the thousands of spots of the varying intensities on the CRT that corresponds to the topography of the sample.

3.2.3 Atomic Force Microscopy (AFM):

Atomic force microscope is one of the most important techniques in modern world. It has many advantages over many other techniques used for characterization of specimen. The important of AFM can be understood by looking at the number of application it has e.g. it can be use in insulator surface topography, charge deposition on insulator, atom by atom deposition, nanometer scale imagine for bio-samples where electron microscope is not suitable for preparatory reasons, measurement of roughness and hardness of specimen etc.

AFM consist of different part as:

1. Cantilever and Tip
2. Deflection sensing system
3. Photodiode
4. Piezoelectric scanner
5. High gain voltage amplifier
6. Vibration isolator

Each of these is integral part of AFM and has some specific role in carrying out measurement.

AFM can be operated in three modes. They are as

1. Cont mode
2. Non- Contact mode
3. Tapping mode

When tip of AFM point over the specimen, there can be either attractive force or repulsive force between the tip atom and atom of the specimen around the tip. If this force is repulsive it is said to be in contact mode when this force is attractive it is said to be non- conduct mode. Figure 3.12 shows the fore vs distance (between tip and the specimen) and point the various mode of the operation applicable on the different position of the curve.

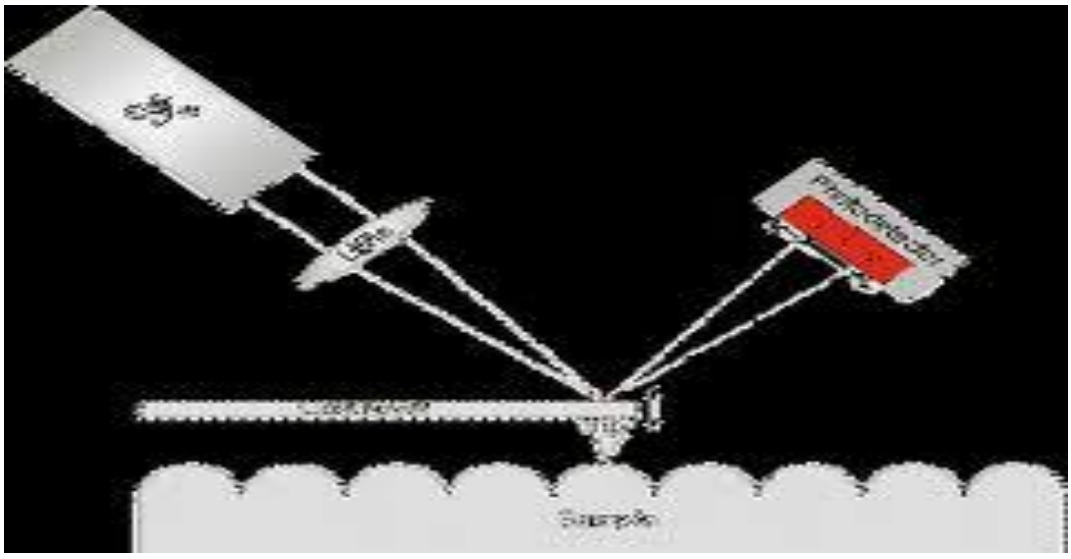

Fig. 3.11 AFM setup

Following Figure shows the schematic diagram of AFM with different part of information about specimen is proceed and finally made available to us.

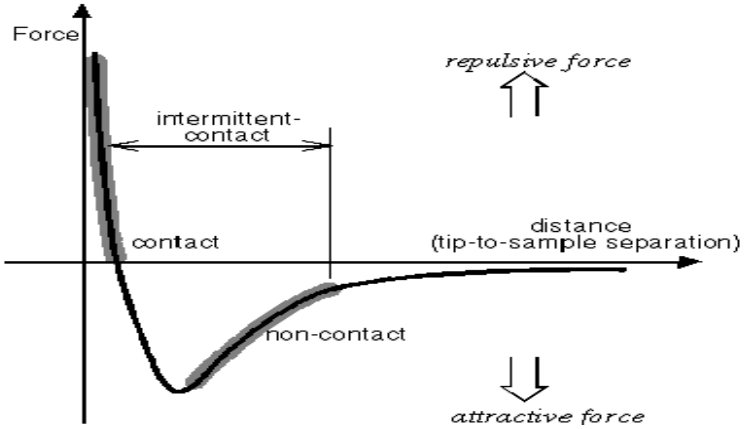

Fig. 3.12 Diagram of Atomic Force Microscope

3.3. Electrical Measurement:

3.3.1 Masking and Electroding:

The annealing the thin film were ground and masked using different graded masked chemical. These masked samples were ultrasonically cleaned to remove any kind of masked material left on the sample. Then silver electrodes were deposited on films phases of the sample and then sample is fired at 300 ^{o}C for 30 mins.

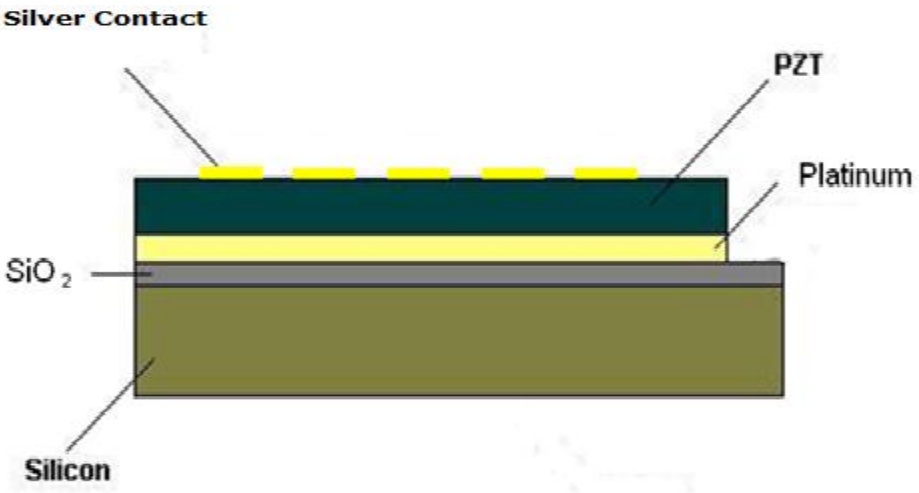

Fig. 3.12 Silver electrode contact

Platform for loading thin films.

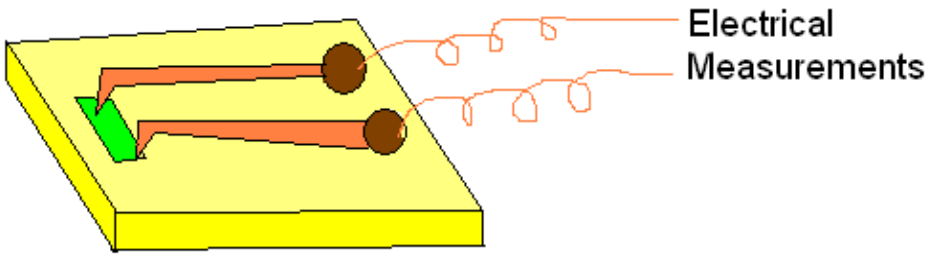

Fig 3.13

3.3.2. Dielectric Measurements

Dielectric measurements of the samples were carried out using computerized measurement set up. This system includes an impedance analyzer model HP 4192 A interfaced to a PC via GPIB interface, a furnace, temperature controller connected to PC via RS 485, sample holder, measurement cable (16048 A test leads) and software. Capacitance (C_p) and dielectric loss (D or Tan δ) of the samples were measured as a function of frequency at fixed temperatures and as a function of temperature at fixed frequencies. Temperature variation of the sample was done using a furnace (from room temperature to 873 K) controlled with computer interfaced temperature controller (± 1 K). Capacitance (C_p) and dielectric loss (D) measurements were used to calculate the real part (ε_r') and Imaginary part (ε_r'') of dielectric constant using following relations.

$$\varepsilon_r' = \frac{C.t}{\varepsilon_0.A} \tag{3.6}$$

$$\varepsilon_r'' = \varepsilon_r' D \tag{3.7}$$

In the above relation t is thickness, A is the area of the electrode made on the sample and ε_0 is the permittivity (8.85×10^{-12} F/m) of free space.

3.3.5. Ferroelectric Measurements:

Ferroelectric hysteresis (*P-E*) loops at room temperature and above room temperature for all samples were performed using a ferroelectric tester (Radiant technologies Precision Premier II). The set up contains a power supply up to 10 kV, main ferroelectric tester, high voltage interface, sample holder and software (includes measurement filters). While performing the measurements the sample holder was kept in silicon oil bath to avoid any sparking or breakdown at high voltage. Ferroelectric tester has the facility to measure the *P-E* loops at different frequencies (0.1 Hz to 1 kHz). Using ferroelectric tester, leakage current and normalized capacitance (*C*) vs. voltage (*V*) measurements was also preformed for the samples.

For temperature variation of the sample, temperature controlled furnace was used. The furnace temperature can be varied from room temperature to 873 K with precision ± 1 K. However *P-E* loops were taken up to maximum temperature 460 K. Above this temperature the silicon oil starts evaporating.

CHAPTER 4

RESULTs AND DISCUSSION OF $PbZrTiO_3$ THIN FILMS

In this chapter we will discuss the $PbZrTiO_3$ thin films data obtained from XRD, AFM, electrical measurement (P-E Loops, I-V, Dielectric constant).

4.1. Structural Analysis of $PbZrTiO_3$:

Fig. 4.1 shows room temperature XRD patterns of PZT thin films deposited by spin coating technique on platinized silicon substrate. Films were pyrolyzed at 350 ^oC and annealed at 200, 400, 550, 600 ^oC for 10 min to analyze the effect of soaking time we kept one film at 600 ^oC for 30 min. It can be seen that as the annealing temperature increased the PZT peaks become gradually more apparent and their intensity is maximum at 600 ^oC. film kept for 30 min at 600 ^oC shows more intense peaks but the intensity of

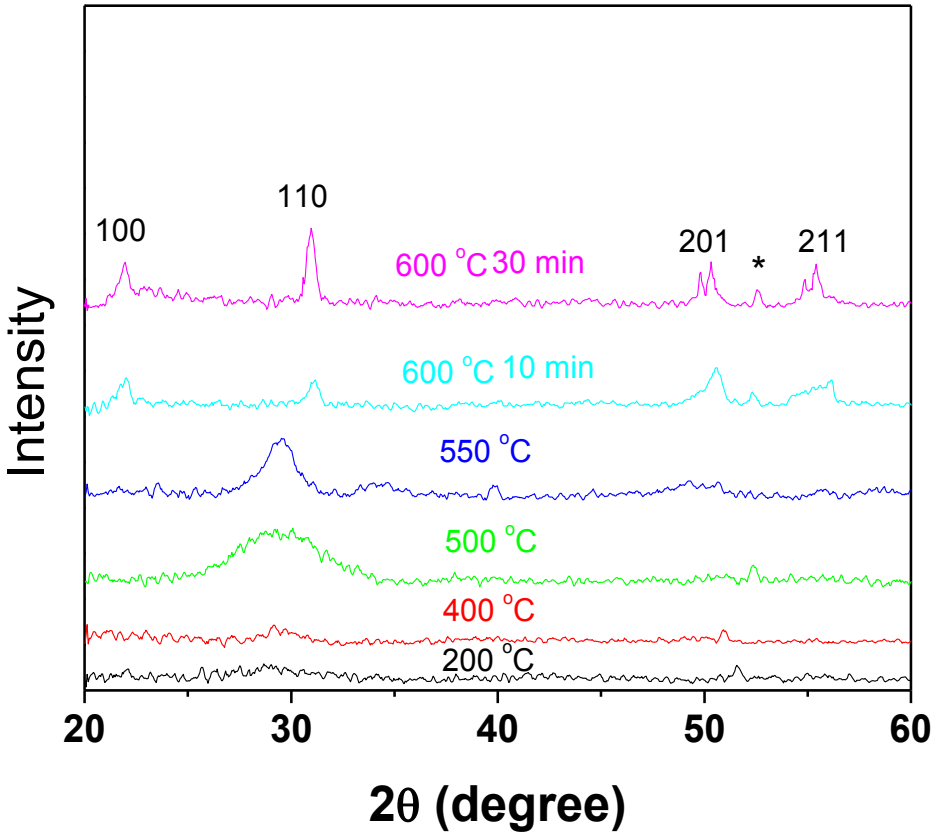

Fig. 4.1 XRD patterns obtained from films pyrolyzed at 350 ^oC and annealed for 10 min at 200, 400,500, 550, 600 ^oC and 30 min at 600 ^oC.

The microstrures shown for the PZT thin films were having nano dimension. A 3D and plane view of the AFM micrographs for all the modified PZTs has been shown and the results are discussed taking into account the morphology, surface smoothness and grain size.

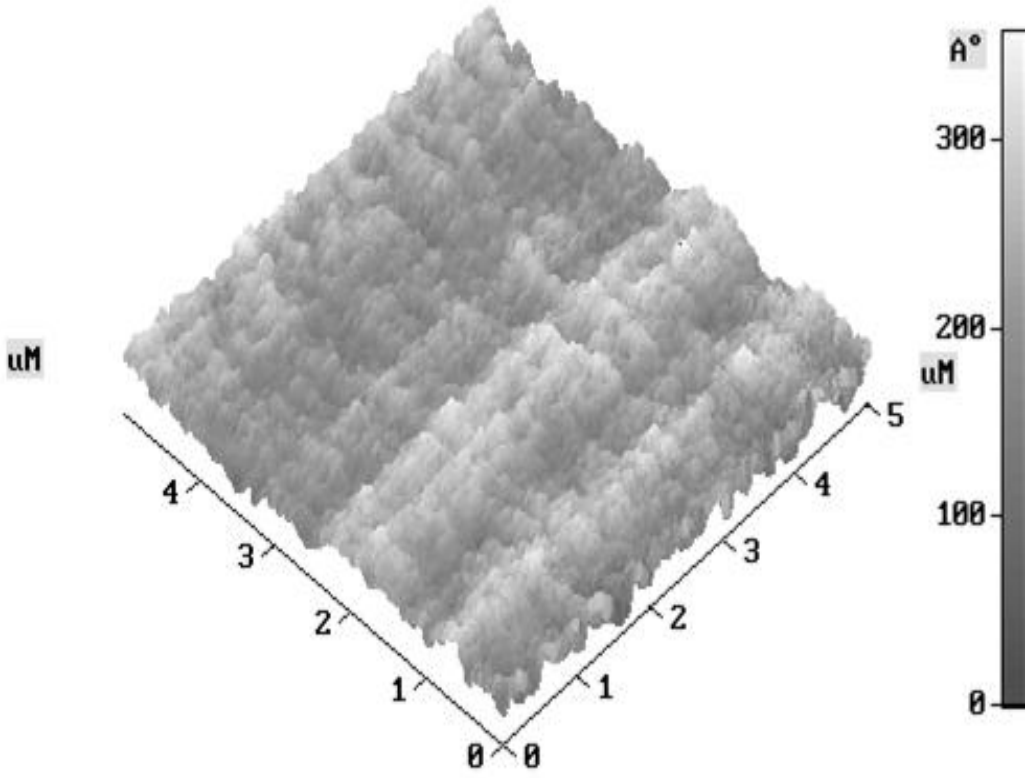

(a)

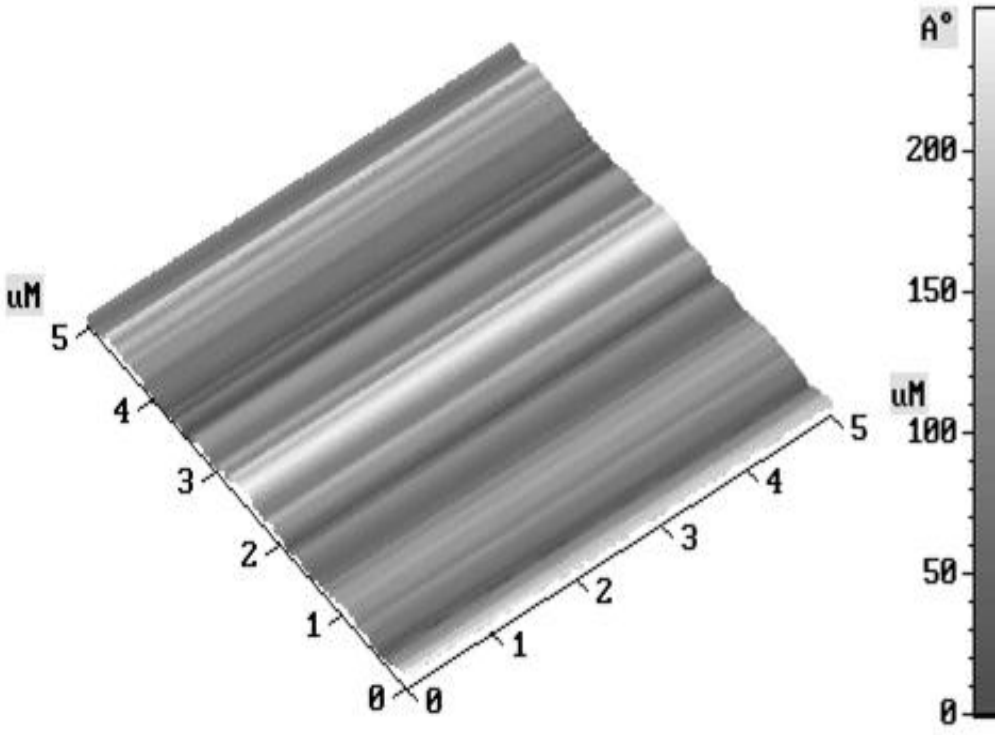

(b)

Fig.4.2. 3-D view of AFM image of the Platinised Substrate (a) Pt/Si<100> and (b) Pt/Si <111>.

AFM data showing surface roughness of the platinised silicon substrates

Substrates (5μm x 5μm)	Average surface roughness (R_a) (nm)	Mean surface roughness (R_{mean}) (nm)
Pt/Si <100>	3.5	21.9
Pt/Si <111>	4.0	12.3

Before depositing thin films of modified PZT, the surface roughness of the substrates was analysed and the results are shown in Table and Fig 4.2. The AFM micrographs (2-D and 3-D view) for the PZT (48/52) on the platinised silicon substrates before depositing PZT (48/52) by sol gel are shown in Fig 4.4 (a, b). The average surface roughness (R_a) in PZT films deposited on Pt/Si <111> by sol gel technique is 0.7 nm. The

growth in the film also looked oriented. The PZT films deposited by sol gel technique on Pt/Si <111> substrates have a surface roughness of 3.8 nm. Thus a larger grain size and smooth nano size surface roughness could be the reason for increase in remnant polarization.

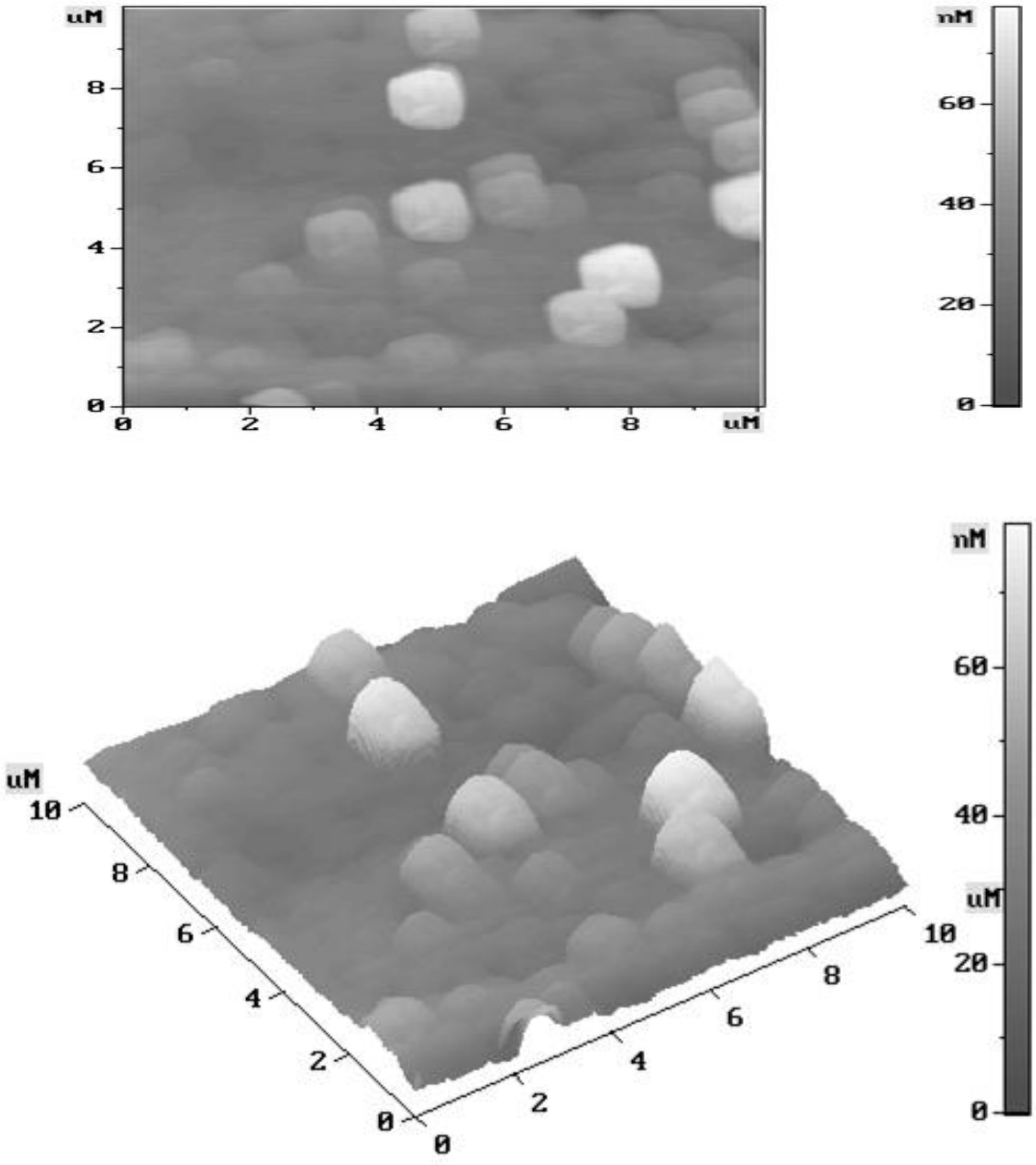

Fig. 4.4. AFM image of the PZT (48/52) thin film deposited on Pt/Si<111>substrate by sol gel technique (i) 2-D view and (ii)3-D view.

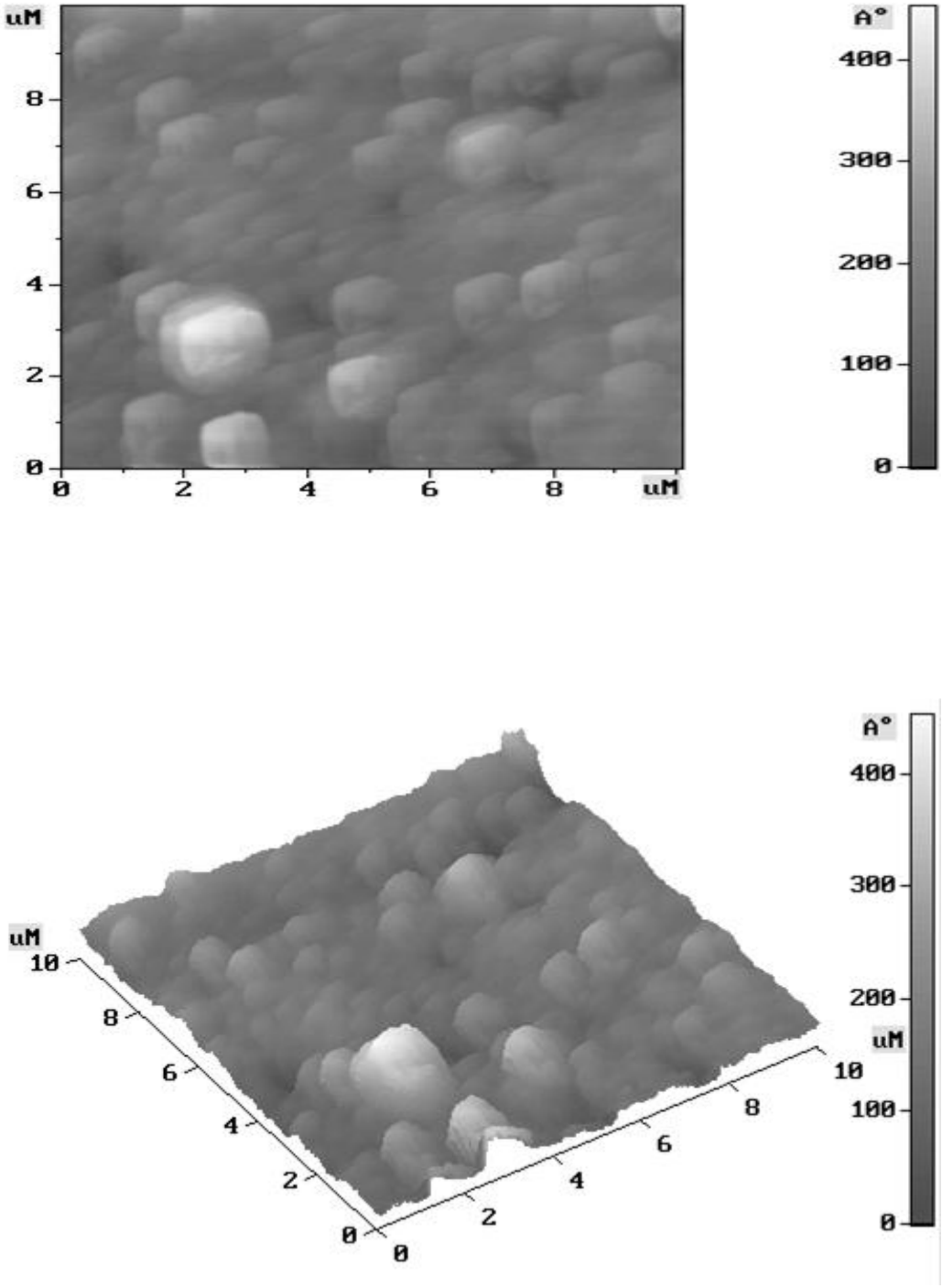

Fig. 4.5. AFM image of the PZT (52/48) thin film deposited on Pt/Si<111>substrate by sol gel technique (i) 2-D view and (ii)3-D view.

4.3 Optical Images of $PbZrTiO_3$:

Fig. 4.6 and 4.7 show optical images of PZT thin films annealed at 600 ^oC for 10 min and 30 min. Both images are taken at 1000 magnification; we can see that film annealed for 30 min is more uniform.

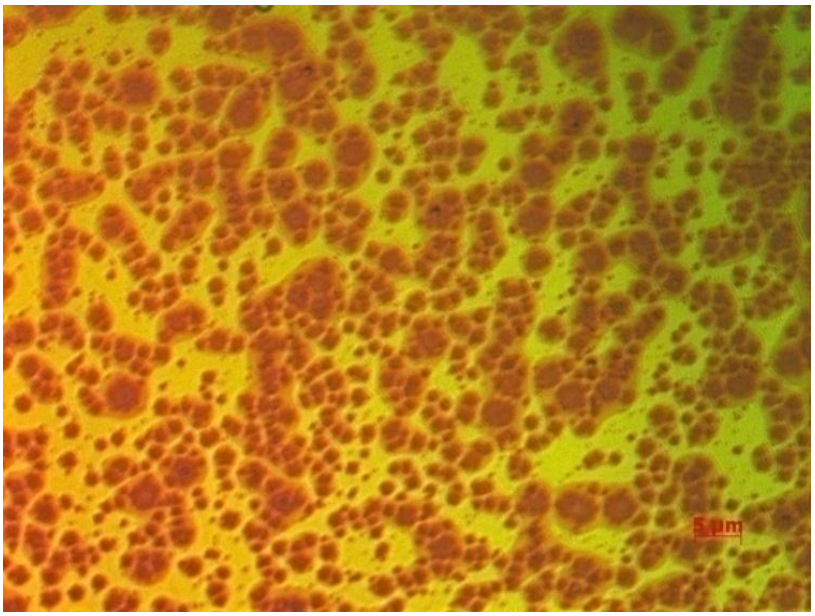

Fig. 4.6 PZT film annealed at 600 ^oC for 10 min

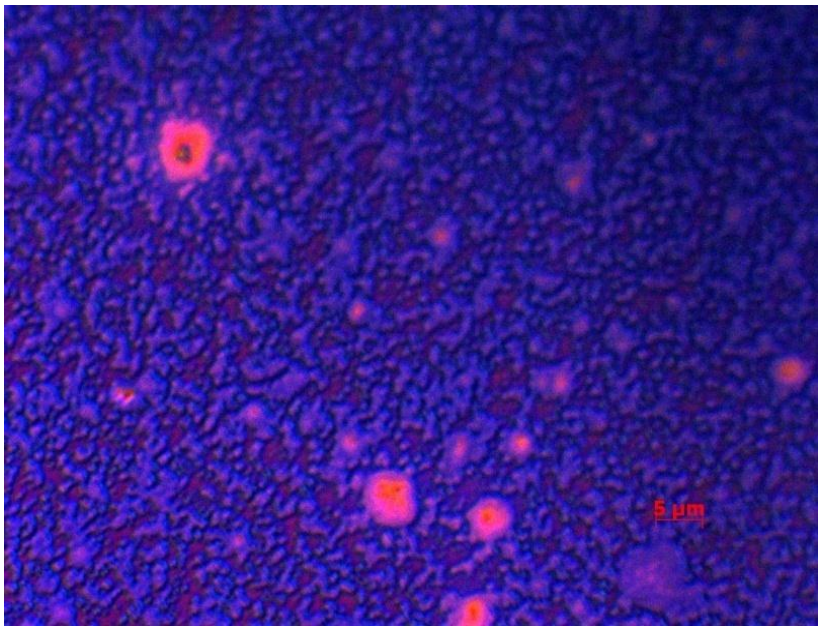

Fig. 4.7 PZT film annealed at 600 ^oC for 30 min

4.4. Electrical Property of PZT Thin films:

4.4.1. P-E Hysteresis loops:

Fig. 4.8 shows room temperature *P–E* hysteresis loops of PZT film annealed at 600 ^{o}C for 30 min at different frequencies. It can be seen that value of remnant polarization (P_R) decreases with the increase of applies field frequency. Coercive field values are found almost same for all loops.

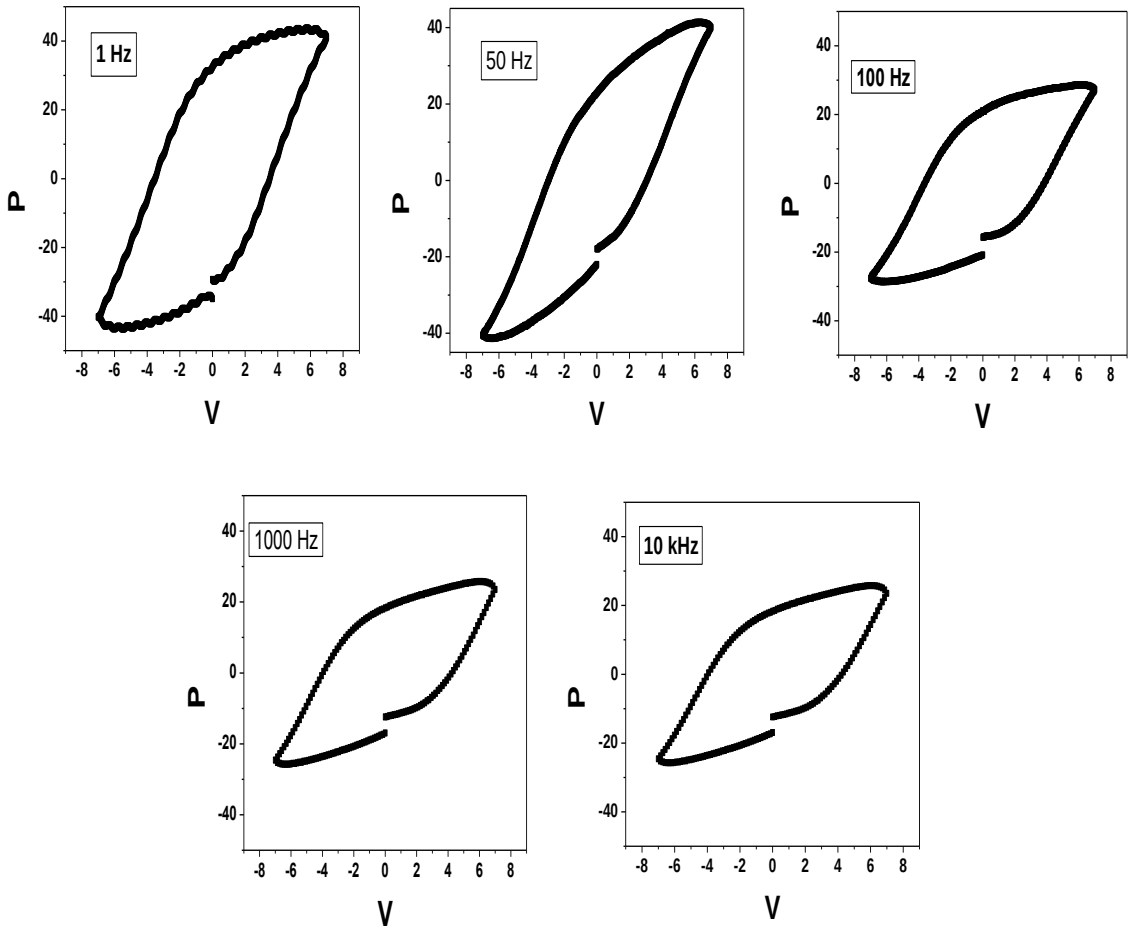

Fig. 4.8 P-E loops at different frequencies

4.4.2. Dielectric Measurement:

Fig. 4.9 shows the dielectric behavior of PZT film annealed at 600 ^{o}C for 30 min with temperature and frequencies. Value of transition temperatures 367 ^{o}C and dielectric

constants 13000 are observed for 10 kHz frequency. The ferroelectric transition temperature was found to be same (T_C) for all frequencies (non-relaxor behavior).

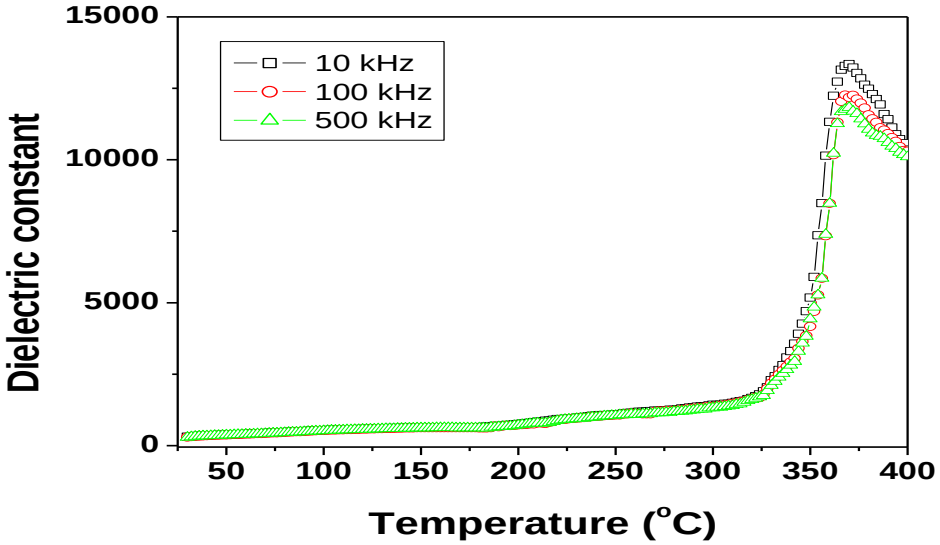

Fig 4.9. Dielectric constant vs temperature for different frequencies, the film

4.4.3. I-V Measurement:

Fig.4.10 shows I-V characteristic plots for as deposited as well as 600 °C annealed PZT thin films. It is found that resistivity of film increases with the increase of crystalline

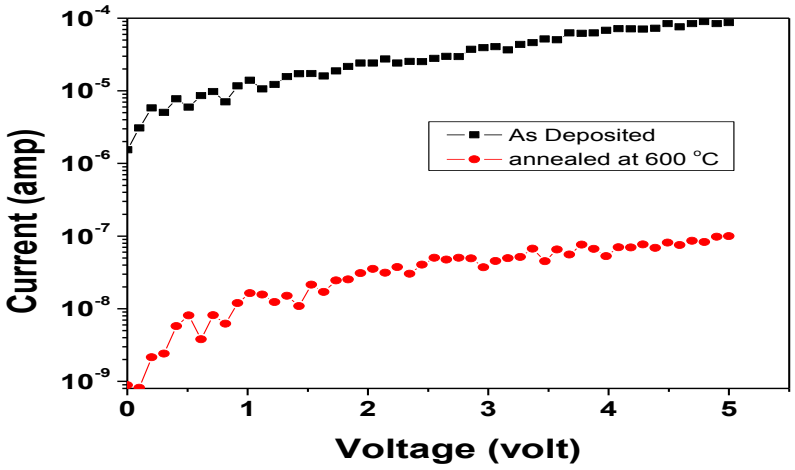

Fig. 4.10 Current vs Voltage at RT for 600 °C annealed PZT

CHAPTER 5

RESULTS AND DISCUSSION OF MULTIFERROIC BF-PZT COMPOSITE THIN FILMS

In this chapter we will discuss BF-PZT heterolayered thin film data obtained from XRD, optical images and electrical characteristic (P-E loops) of $BiFeO_3$-$PbZrTiO_3$ thin film.

5.1. Structural Analysis of $BiFeO_3/PbZrTiO_3$ Film

Fig.5.1 shows room temperature XRD patterns of BF-PZT thin films deposited by spin coating technique on platinized silicon substrate. Films were pyrolyzed at 350 ^oC and annealed at 500 and 600 ^oC for 10 min to analyze the effect of soaking time we kept one film at 600 ^oC for 30 min. It can be seen that as the annealing temperature increased the BF-PZT peaks become gradually more apparent and their intensity is maximum for 600 ^oC annealed film.

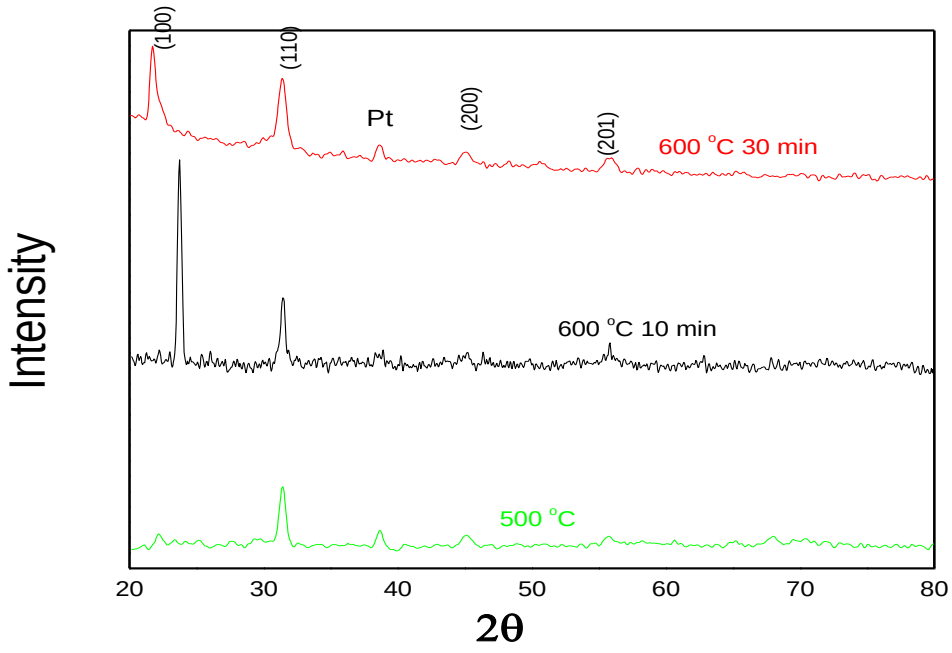

Fig. 5.1 films pyrolyzed at 350 ^oC and annealed for 10 min at 500,600 ^oC and 30 min at 600 ^oC.

5.2. Optical Images of BiFeO3/$PbZrTiO_3$ Films

Fig. 5.2 (a) and (b) optical images of BF-PZT thin films annealed at 600 ^{o}C for 10 min and 30 min. All images are taken at 1000 magnification; we can see that film annealed for 30 min is more uniform than other film.

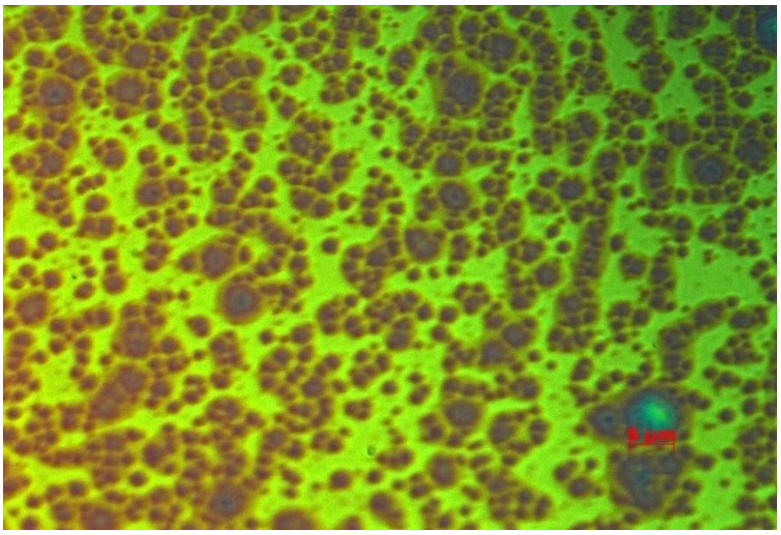

Fig. 5.2 (a) BF-PZT Image annealed for 10 min at 600 ^{o}C

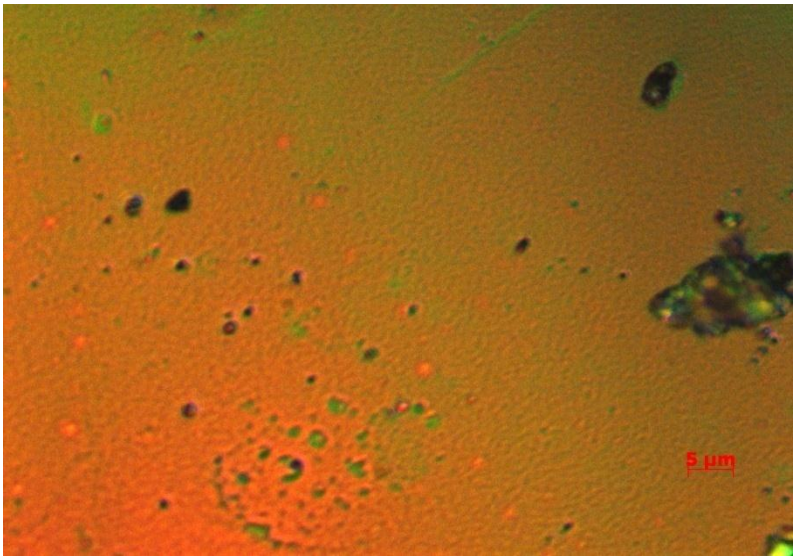

Fig. 5.2 (b) BF-PZT image annealed for 10 min at 600 ^{o}C

5.3. Electrical Property of $PbZrTi\ O_3/BiFeO_3$:

5.3.1. P-E Hysteresis loop:

Fig. 5.3 shows variation of polarization applied the electric field. The quantities of spontaneous polarization and coercive fields, in the direction of the applied electric field, we can be easily and reliably extracted. We found for our $PbZrTiO_3$-$BiFeO_3$ poly crystalline at room temperature a remnant polarization P 3.5 μC cm^{-2} and a coercivity of 2 kV/cm. saturation polarization is close to 8.5 μC cm^{-2}. This value is in good agreement with theoretical predictions and thin film data.

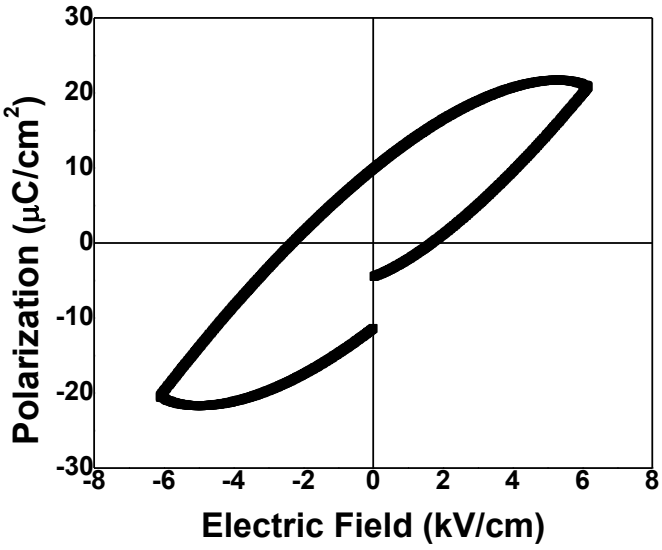

Fig. 5.3 P-E hysteresis loops of $BiFeO_3$-$PbZrTiO_3$ film annealed at 600 ^{o}C for 30 min

CHAPTER 6

SUMMARY, CONCLUSION AND FUTURE SCOPE

This chapter highlights the salient features and major conclusions of present study and scope of future work in PZT, BF and BF-PZT thin films.

6.1. Summary, Conclusion

In present work, PZT ($PbZrTiO_3$) have been studied for their structural, microstructural, dielectric, ferroelectric, and electrical properties. The summary of our findings on these systems are given as follows.

6.1.1. $PbZrTiO_3$ thin films

- All films are deposited by Sol-Gel technique.
- X-rd pattern confirm that 600 ^oC films are more crystalline.
- Optical images of the films show that films are uniform.
- The AFM micrograph reveals that the PZT thin film is well crystallized and cracks free, and has nearly uniform grain distribution. The mean grain size of surface of thin film is 10 nm. The root-mean-square (rms) roughness and mean roughness is 2.2 nm and 1.78 nm respectively.
- Remnant polarization (P_R) decreases with the increase of applies field frequency. Coercive field values are found almost same for all loops.
- Transition temperatures 367^oC and dielectric constants 13000 are observed for 10 kHz frequency. The ferroelectric transition temperature was found to be same (T_C) for all frequencies.
- It is found that resistivity of film increases with the increase of crystallinity.

6.1.2. $BiFeO_3$-$PbZrTiO_3$ thin film

- All films are deposited by Gol-Gel technique.
- X-rd pattern confirm that 600 ^oC films are more crystalline.
- Optical images of the films show that films are uniform.
- All fims are poly crystaline at room temperature a remnant polarization P 3.5 μC cm^{-2} and a coercivity of 2 kV/cm. saturation polarization along the direction is close to 8.5 μC cm^{-2}.

6.2. Direction for Future Work

Following are the directions for the future work that has evolved out of understanding gained on the subject during the course of present studies.

- Magnetic measurements of BF and BF-PZT thin films can be performed to analyze magnetic behavior.
- Deposition techniques like spray pyrolysis and dip coating can be try.
- Multiferroic properties of BF and BF-PZT thin films can be performed to analyze magneto-electric behavior.

References

1. J. C. Maxwell, *Phil. Trans. R. Soc. Lond.* **155,** 459–512 (1865).
2. L. D. Landau, & E. M. Lifshitz, *The Classical Theory of Fields* 2nd edn (Pergamon, London, 1962).
3. P. Curie, *J. Physique* **3**, 393 (1894).
4. L. D. Landau and E. M. Lifshitz, *Electrodynamics of continuous media*. (Fizmatgiz, Moscow, 1959).
5. Anupinder Singh, Arti Gupta and Ratnamala Chatterjee, Applied Physics Letters 93, 022902 (2008).
6. Arti Gupta, Ratnamala Chatterjee, Appl. Phys. 106,024110(2009).
7. L.G. Tejuca, J. Less, Common Met. 146 (1989) 251.
8. T. Arakawa, H. Kurachi, J. Shiokawa, J. Mater. Sci. 20 (1985) 1207.
9. F. Scott, *Rep. Prog. Phys.* **42**, 1055 (1979).
10. H. Schmid, *Introduction to the proceedings of the 2nd international conference on* J. P. Rivera, *Ferroelectrics* **161**, 165 (1994). *magnetoelectric interaction Phenomena in crystals, MEIPIC-2. Ferroelectrics* **161**, 1–28 (1994)
11. J. -P. Rivera, *Ferroelectrics* **161**, 165 (1994).
12. J. Wang, J. B. Neaten, H. Zheng, V. Nagarajan, S. B. Ogale, B. Liu,1 D. Viehland, V. Vaithyanathan, D. G. Schlom, U. V. Waghmare, N. A. Spaldin, K. M. Rabe, M. Wuttig, R. Ramesh, *Science* **299**, 1719 (2003).
13. T. Kimura, *Nature* **426**, 55 (2003).
14. W. Eerenstein, N. D. Mathur and J. F. Scott, *Nature* **442**, 759 (2006).
15. S.W.Cheong and Maxim Mostovoy, *Nature Mater.* **6**, 13 (2007).
16. J. F. Scott, *Nature Mater.* **6**, 256 (2007).
17. H. Béa, M. Gajek, M. Bibes and A. Barthélémy, *J. Phys.:Condens. Matter* **20**, 434221 (2008).
18. S. J. Gong and Q. Jiang, *Phys. Lett. A* **333**, 124 (2004).
19. J. H. Van Vleck, *The Theory of Electric and Magnetic Susceptibilities* (London: Oxford University Press,1932).
20. D. Khomskii, *Physics* **2**, 20 (2009).
21. N. Hur *et al., Nature* **429**, 392 (2004).

22. A. M. J. G.van Run, D. R. Terrell, & J. H. Scholing, *J. Mater. Sci.* **9**, 1710 (1974).
23. J. Ryu, A. Va´squez Carazo, , K. Uchino, & H.-E. Kim, *Jpn. J. Appl. Phys.* **40**, 4948 (2001).
24. N. Cai, C.-W. Nan, J. Zhai, & Y. Lin, . *Appl. Phys. Lett.* **84**, 3516 (2004).
25. G. Srinivasan *et al., Phys. Rev. B* **65**, 134402 (2002).
26. A.J. Moulson and J.M. Herbert, "Electroceramics : Materials, Properties and Application" Chapman and Hall (1990).
27. L.C. Klein, in *"*Sol-gel Technology for Thin Films, Fibers, Preforms, Electronics, and Specialty Shapes*"* (Noyes Publications, Park Ridge, New Jersey, 1988).
28. K.D Budd, S.K. Dey and D.A. Payne, *Brit. Ceram. Proc*. 36 (1985) 107.
29. G. Catalan and J. F. Scott, *Adv. Mater.* **21**, 2463 (2009).
30. J.D. Mackenzie and Y. Xu, *J. Sol-Gel Sci. Technol.*, 8 (1997) 673.
31. R. Thomas, S. Mochizuki, T. Mihara and T. Ishida, *Thin Solid Films*, 443 (2003) 14.
32. C. Zhu, Z. Yong, Y. Chentao and Y. Bangchao, *Mater. Sci. Eng. B*, 123 (2005) 143.
33. Z. Kighelman, D. , A. Seifert, S. Gentil, S. Hiboux and N. Setter, *Mater. Res. Soc. Symp. Proc.*, 596 (2000) 523.
34. J.G. Cheng, J. Tang, X.J. Meng, S.L. Guo, J.H. Chu, M. Wang, H. Wang and Z. Wang, *J. Amer. Ceram. Soc.*, 84 (2001) 1421.
35. V. Joshi, D. Roy and M.L. Mecarthey, *Appl. Phys. Lett.*, 63 (1993) 1331.
36. M. Pereira and M.J.M Gomes, *J. Eur. Ceram. Soc.* 25 (2005) 2285.
37. R.J. Ong, T. A. Berfield, N. R. Sottos and D. A. Payne, *J. Eur. Ceram. Soc.*, 25 (2005) 2247.
38. A. Montenero, M. Canali, H. Gnappi, D. Bersani, P.P. Lottici, P. Nunziante and E. Traversa, *Appl. Organometal. Chem.*, 11 (1997) 137.
39. A. Li, C. Ge, P. Lü, D. Wu, S. Xiong and N. Ming, *Appl. Phys. Lett.*, 70 (1997) 1616.
40. C.J. Kim and Y.K. Lee, *Mater. Sci. Eng.* B, 122 (2005) 12.
41. D.L. Segal, *J. Non-Crystalline Solids*, 63 (1984) 183.
42. A.C. Pierre, in *"*Introduction to Sol-Gel Processing*"* (Kluwer Academic Publishers, Boston, 1998).
43. B.A. Tuttle and R.W. Schwartz, *MRS Bull.*, 21 (1996) 49.

44. C.J. Brinker, in *"*Sol-Gel Science: the Physics and Chemistry of Sol-Gel Processing*"* (Academic Press, London, 1990).
45. R.W. Schwartz, R.A. Assink, D. Dimos, M.B. Sinclair, T.J. Boyle and C.D. Buchheit, *Mater. Res. Soc. Symp. Proc.*, 361 (1995) 377.
46. G. Yi and M. Sayer, *J. Sol-Gel Sci. Technol.*, 6 (1996) 65.
47. Y.T. Kwon, I.-M. Lee, W.I. Lee, C.J. Kim and I.K. Yoo, *Mater. Res. Bull.*, 34 (1999) 749.
48. R.A. Roy, K.F. Etzold and J.J. Cuomo, Mater. Res. Soc. Symp., 200 (1990) 141.
49. W.A. Geideman, *IEEE UFFC*, 38 (1991) 704.
50. A.F. Tash and L.H. Parker, IEEE, 77 (1989) 374.
51. M. Vopsaroiu, J. Blackburn, A. Muniz-Piniella, and M. G. Cain, *J. Appl. Phys.* **103**, 07F506 (2008).
52. R. Ramesh and N. A. Spaldin, *Nature Mater.* **6,** 21 (2007).
53. P. Ravindran, R. Vidhya, A. Kjekshus and H. Fjellvag, *Phys. Rev. B* **74,** 224412 (2006) and references therein.
54. H. Bea, M. Bibes, A. Barthe´le´my, K. Bouzehouane, E. Jacquet, A. Khodan, J.-P. Contour, *Appl. Phys. Lett.* **87**, 072508 (2005).
55. H. Schmidt, Ferroelectrics 162 (1994) 317.
56. N.A. Hill, J. Phys. Chem. B 104 (2000) 6694.
57. L.C. Klein, in *"*Sol-gel Technology for Thin Films, Fibers, Preforms, Electronics, and Specialty Shapes*"* (Noyes Publications, Park Ridge, New Jersey, 1988).
58. K.D Budd, S.K. Dey and D.A. Payne, *Brit. Ceram. Proc*. 36 (1985) 107.
59. J.D. Mackenzie and Y. Xu, *J. Sol-Gel Sci. Technol.*, 8 (1997) 673.
60. C. Zhu, Z. Yong, Y. Chentao and Y. Bangchao, *Mater. Sci. Eng. B,* 123 (2005) 143.
61. D.L. Segal, *J. Non-Crystalline Solids,* 63 (21984) 183.
62. A.C. Pierre, in *"*Introduction to Sol-Gel Processing*"* (Kluwer Academic Publishers, Boston, 1998).